Chapter 4: Results and Analysis

This chapter presents the results from the experiments that were outlined in Chapter 3. Tests were carried out in the wind tunnel to observe flow and heat transfer in the tip region with different tip geometries. The results are presented in the dimensionless form of static pressure coefficient, adiabatic effectiveness, and cooling effectiveness.

Static pressure measurements were made on the shroud in and around the tip region. Each pressure measurement on the shroud is reported as a pressure coefficient which is defined as

$$C_p = \frac{P_{s,\,local} - P_{s,\,inlet}}{P_{dyn,\,inlet}} \tag{4-1}$$

where $P_{s,local}$ is the static pressure measured at a shroud location; $P_{s,inlet}$ is the static pressure measured 0.54 chords upstream (along the x-axis) of the midspan stagnation; and $P_{dyn,inlet}$ is the average dynamic pressure measured at seven locations across the y-direction at 0.54 chords upstream of the center blade stagnation location.

To measure film cooling effects of the microcircuit and dirt purge holes on the tip we measured the temperatures along the foam blade tip, T_{aw}, with an infrared camera. These temperatures are reported as a dimensionless term called adiabatic effectiveness which is defined as

$$\eta = \frac{T_\infty - T_{aw}}{T_\infty - T_c} \tag{4-2}$$

where T_∞ is the mainstream temperature, T_c is the coolant temperature, and T_{aw} is the adiabatic wall temperature. If $\eta = 1$ at a certain location, then $T_{aw} = T_c$, and the blade is perfectly cooled. If, at another location, $\eta = 0$, then $T_{aw} = T_\infty$, and the blade is not cooled at all. Thus, the adiabatic effectiveness, η, is a measure of how effectively the blade tip is cooled by injected flow.

To observe internal convection effects of the microcircuit in addition to film cooling effects, surface temperature measurements were made on an alumina tip model with Biot number matched to the engine conditions. These temperature measurements are reported in a dimensionless term called cooling effectiveness. Similar to adiabatic effectiveness, cooling effectiveness is calculated as

$$\phi = \frac{T_\infty - T_m}{T_\infty - T_c} \tag{4-3}$$

where T_m is the metal temperature. This is the temperature measured experimentally on the alumina tip surface. As with the adiabatic case, T_∞ is the mainstream temperature, and T_c is the coolant temperature entering the plenum (inlet to the microcircuit).

Before experimental results are given, the first section provides a discussion of the scaling techniques used to correlate engine conditions to tunnel conditions. Based on this scaling, the experimental test matrix is presented in the second section. The following section presents temperature and pressure measurements that were made in the wind tunnel as contours of pressure coefficients and effectiveness levels. The pressure coefficients for the case of a flat blade tip are shown first providing a background of the basic flow phenomena. Then, results are presented for blowing from the dirt purge holes alone, followed by results for the case with cooling air coming from the dirt purge holes and the microcircuit. The last section of this chapter provides a brief discussion on how this data can be used in a complete heat transfer analysis of the blade.

4.1 Engine Scaling of Low Speed Wind Tunnel Measurements

This section discusses the scaling techniques that were used to match the measurements made at tunnel conditions to engine conditions. Before engaging in this discussion, it may be useful to review basic terminologies regarding turbine blade geometry. Figure 4-1 shows the basic features of a blade profile as they are angled with respect to the tunnel. A Cartesian coordinate system labeled x, y, and z is oriented with respect to the wind tunnel axis, while a second system with directions X, Y, and Z is placed at the stagnation location of the blade at the midspan with the X axis parallel to the flow direction. The pitch, P, is the distance between each blade that is parallel to the Y-axis. The axial chord, B_X, is the blade length along the axial or X direction, and the true chord, C, is the straight line distance from the stagnation point on the leading edge to the trailing edge. The blade angle, ϕ, is the angle between the true chord and the X-axis. The angle of incoming flow with respect to X is labeled as θ, the entrance angle. Not shown in Figure 4-1 is the span, S, which is the length of the blade in the Z direction. U, V, and W are velocity vectors that correspond to the X, Y, and Z directions, respectively.

These experimental studies are an attempt to replicate conditions during actual engine operation in the confines of a controlled environment. Such an environment includes

representative conditions to be observed through large scale testing. Therefore, the blade geometry was built to a larger scale, so that good measurement resolution could be obtained on the tip surface. However, it is extremely difficult and impractical to match actual engine temperatures and velocities at a large scale while enabling measurements to be aquired. Instead, engine Reynolds numbers are matched in a low speed wind tunnel with the following relationship

$$\mathrm{Re}_e = \frac{\rho_e U_e C_e}{\mu_e} = \frac{\rho_t U_t C_t}{\mu_t} = \mathrm{Re}_t \qquad (4\text{-}4)$$

where "e" denotes engine conditions and "t" denotes test conditions. Based on the true chord, the engine Reynolds number to be matched is 2.1 x 10^5. The tunnel operates at ambient conditions, so density, ρ, and viscosity, μ, are fixed. This leaves blade scaling and inlet velocity, U, as parameters that can be modified to match an engine Reynolds number. The true chord was designated as the reference length, so the ratio of the test chord, C_t, to the engine chord, C_e, is the scaling factor. The size of the scaling factor determines measurement resolution but is restricted by the size of the wind tunnel. Because it is important to obtain periodic flow conditions, three blades are required to create two full air passages. This constraint, coupled with the size of the wind tunnel passage, limited the blade scaling factor to 12. At this scale there is an achievable tunnel velocity that matches the engine Reynolds number.

In addition to matching Reynolds number, the pressure distribution around the blade had to be matched to engine conditions because the tip gap flow is dominated by the pressure difference across the tip gap. Therefore the blade cross-section was redesigned for low speed testing. Figure 4-2 compares the low speed blade shape that was designed by Praisner [2002] of Pratt and Whitney to match the pressure distribution around a blade in high speed engine conditions.

Though the engine Reynolds number is matched by the tunnel, calculations by Blair [2002] at Pratt & Whitney show that blowing ratios would be scaled by a factor of 1.79 because of differences in the properties of air at these conditions. Detailed calculations arriving at this figure are included in Hohlfeld [2003]. Table 4-1 summarizes the flows that were used in the wind tunnel compared to those in an engine. A discussion of the blowing ratios that were simulated will be included in the next section, which presents the experimental test matrix.

4.2 Experimental Test Matrix for Tip Testing

This section provides the test cases in which temperature and pressure were measured. Factors that were varied include geometry, material, tip gap height, and blowing ratio. Table 4-2 summarizes all of the different cases that were experimentally simulated. Three basic geometries were tested: a blade with a flat tip surface and no film cooling holes, a blade with dirt purge holes, and a blade with dirt purge holes and microcircuit film-cooling holes. The blade material was varied only for cases with the microcircuit, and as discussed in Chapter 1 provides an indication of the conductive effects of an actual turbine blade. Surface temperature measurements were made on a foam blade so that effectiveness could be calculated with an adiabatic surface. Temperatures on a second material, alumina, were measured so that the internal effects of the microcircuit cooling could be assessed.

The same blade model was used for all of the tests with the use of tape when necessary for blocking off the dirt purge or microcircuit film-cooling hole exits. For the flat tip case, the entire dirt purge cavity was covered in such a way that the blade tip surface was completely flat, and only static pressure measurements on the shroud were taken. The foam model was used although the material is irrelevant for pressure measurements. It is assumed that the surface roughness of both the alumina and foam models is smooth enough that the flow field is not noticeably affected

The tip gap height was altered for all three of the geometries used. Measurements were taken at tip gap heights of 0.54% and 1.63% of the blade span. Provided by Pratt & Whitney, these gap sizes were based on a range observed from actual engine conditions. The 0.54% and 1.63% gap heights correspond to actual engine gaps of 0.248 mm (0.010 in) and 0.750 mm (0.030 in), respectively. To provide a frame of reference, the smaller gap size for an engine is about the thickness of two pieces of paper. Our tests were conducted on a 12X scale model, so the tip gap sizes were 3 mm (0.118 in) and 9 mm (0.354 in). For the remainder of this report, the 3 mm gap will be referred to as the small tip gap, and the 9 mm gap will be called the large tip gap.

For the dirt purge geometry and the dirt purge with microcircuit geometry, the amount of coolant exiting the blade was varied. The blowing ratio is the flowrate of coolant air exiting the

blade expressed as a percentage of the flowrate of air through one full blade passage. A passage is the region between the stagnation lines of two blades or, in other words, the rectangular region defined by the pitch and the span. For the case with the dirt purge and microcircuit injection, tip adiabatic surface temperatures and shroud static pressures were measured at blowing ratios of 0.5%, 1.0%, 1.5%, and 2.0%. In the case with dirt purge injection, the blowing ratios used were 0.10%, 0.19%, 0.29%, and 0.38%. Based on computational predictions made by Hohlfeld [2003], the 0.19% and 0.29% blowing ratios represent the amount of flow that exits the dirt purge holes when the dirt purge holes and microcircuit are flown together at blowing ratios of 1.0% and 1.5%. The 0.10% and 0.38% cases are extrapolations to allow correlation between blowing ratio and film cooling effectiveness. The experimental results are grouped by geometry and presented below starting with the flat tip case.

4.3 Static Pressure Measurements for the Flat Tip Case

A blade with a flat tip and no coolant flow was the first to be tested in the tunnel. This simple geometry would provide a baseline case so that the effects from the coolant flows and geometries tested later could be isolated. This baseline case will also serve as a benchmark for comparison with results in open literature to date. Good agreement between the baseline case and results from similar studies may lend validity to other findings in this research.

Static pressure measurements on the shroud are reported as C_p which is defined by Equation 4-1. Local pressures on the shroud are typically lower than the inlet static pressure because the tip is a region of high flow velocities. For this reason, C_p values are typically large negative numbers. The larger the absolute magnitude of C_p, the lower the local pressure is relative to the inlet static pressure. With this in mind, the pressure contours shown in Figure 4-3 provide interesting insights to the flow in the tip region. The black outline indicates the location of the blade in relation to the shroud contour map.

The contour for a small tip gap in Figure 4-3a shows a low pressure region near the blade midchord which corresponds to C_p = -10. This low pressure region indicates the higher velocities of the tip leakage. Near this leakage and just off the suction side is an even lower pressure region which indicates the presence of the tip leakage vortex observed by Bindon [1989], Prasad [1999], and others in open literature. This vortex was also predicted by Hohlfeld

[2003] for the same blade profile that was used in these experiments. In Figure 4-3b, the midchord leakage appears to increase with a larger tip gap as shown by the low pressure area on the midchord. From the small to large tip gap, the magnitude of C_p at the midchord increases from -10 to -14. According to Bindon, the velocity difference between this midchord tip leakage and the mainstream flow causes the tip leakage vortex, yet the apparent increase in midchord leakage shown here does not appear to significantly alter the low pressure region indicating the tip leakage vortex. It is possible that the tip leakage vortex does in fact increase but may be displaced from the shroud. This could cause the low pressure region to remain unchanged even though the size of the vortex increased. Hohlfeld [2003] shows that the tip leakage vortex is located farther from the shroud with a large tip gap than with a small tip gap.

The next section presents results with blowing from the dirt purge holes. It will be shown that with repeated measurements there actually is a slight difference between tip gaps in the low pressure zone that indicates the tip leakage vortex.

4.4 Dirt Purge Case

The dirt purge geometry is intended to exhaust dirt and dust particles from a turbine blade, so that smaller film cooling holes do not become clogged. This study aims to observe flow field and heat transfer effects in the tip region with dirt purge blowing. With cooling air injected from the dirt purge holes, we made static pressure measurements on the shroud and adiabatic surface temperature measurements on the tip surface. Measurements were made at large and small tip gap heights and at four different blowing ratios. This section presents and discusses these results starting with the C_p distributions on the shroud. Secondly, the η distributions are assessed.

Shroud Pressure Distribution Results. Figure 4-4 shows distributions of pressure coefficients on the shroud for a large tip gap at four blowing ratios from the dirt purge. The baseline case of a flat tip with no blowing on a large tip gap is repeated here for comparison. There are essentially no effects from the dirt purge holes on locations away from the leading edge. The low pressure region at the midchord appears to increase when the blowing ratio reaches 0.19%, but for the 0.38% case this region returns to the size of that in the baseline case.

This suggests that the variation is not caused by dirt purge blowing but by variation between experiments which is within the uncertainty reported in the previous chapter.

Examining the leading edge region, the effects of dirt purge blowing at 0.10% are hardly visible when compared to the baseline case. In the immediate vicinity of the dirt purge holes, there are no major effects, but the pressure contours just downstream of the holes on the suction side of the blade creep towards the leading edge. This may more easily be noticed by examining the orientation of the contours inside the tip gap immediately downstream of the dirt purge cavity. In the baseline case, these contours are normal to the flow direction. In the case of 0.10% blowing, the contours become angled toward the flow. This trend continues into the 0.19% case, and we begin to see a region of lower pressure form immediately behind the dirt purge holes. The dirt purge holes inject a jet of air into the tip gap region, which carries greater momentum at higher blowing ratios. This jet of air blocks the leakage flow and develops a wake of low pressure downstream.

When the blowing ratio increases to 0.29%, we see the pressure downstream of the dirt purge holes continue to drop, but we also see a new formation further upstream. A small spot of low pressure forms next to the leading dirt purge hole on the pressure side. This spot is also present in the 0.38% case and may indicate a circulation of air coming off of the first dirt purge jet. This circulation is similar to the horseshoe vortex described by Sgarzi and Leboeuf [1997]. The horseshoe vortex forms around a jet of air injected normal to the flow. In the case of a dirt purge jet, perhaps the vortex is only noticeable on the pressure side because air is pulled away to the suction side before it can circulate.

Figure 4-5 shows the pressure contours on the shroud for a small tip gap with dirt purge blowing. If the influence of the dirt purge blowing is limited to the area of the shroud above leading edge, the cases in Figure 4-4 and Figure 4-5 can be used to further observe the effect of tip gap height on the tip leakage vortex. The change in blowing ratio does not seem to affect the low pressure region indicating the tip leakage vortex, so we have five cases at each tip gap size to show a trend. In the tip leakage vortex from a large tip gap, the lowest C_p values range between -11 and -13, yet for the small tip gap C_p ranges from -9 to -11 (not including the baseline case). This suggests that, even for the range of tip gap sizes tested here, there is a slight trend that shows the tip leakage vortex increases with tip gap height.

Looking back to the leading edge region, there is a more significant effect from dirt

purge blowing with a small tip gap than with the large tip gap. As with the large tip gap, we see a low pressure area forming on the shroud downstream from the dirt purge holes as the blowing ratio increases. At the 0.19% blowing ratio, we see two regions of lower pressure forming around the dirt purge holes, which indicate higher velocities. These regions become more defined as the blowing ratio increases. As the pressure in these regions decrease with increasing blowing ratio, a region of high pressure forms between them. This region, in which $C_p = -3$ for the baseline case, now has $C_p = 0$. The coolant exits the dirt purge holes with enough momentum to impact the shroud upon which it flows outward and along the shroud. The dirt purge flow maintains a high velocity parallel to the shroud as indicated by the two low pressure regions. We would expect to observe a region of high static pressure at the points of impact, but these points are most likely so localized that they are not resolved by the placement of static pressure taps on the shroud. A high pressure region exists between the points of impact and is caused by the two dirt purge jets stagnating over the cavity. Hohlfeld [2003] was able to computationally illustrate this phenomenon by calculating velocity vectors in a cross section of the dirt purge cavity. These results are shown in Figure 4-6. Velocity vectors indicate that coolant from the dirt purge holes are turned 90° at the shroud. The turned flow from one dirt purge hole stagnates against the turned flow from the other and creates a circulating flowfield in the middle of the dirt purge cavity.

In the small tip gap cases with 0.19%, 0.29%, and 0.38% blowing ratios, there appears to be higher pressures on the pressure side of the tip gap near the leading edge. Air that passed across the leading edge in the baseline case is now blocked by the dirt purge jets. This air stagnates causing the high pressure zones on the pressure side. This high pressure zone is most observable at the 0.19% blowing ratio. It is still present at the higher blowing ratios, but the low pressure regions from the dirt purge jets reduce the area of stagnation. It is likely that this stagnating air is diverted downstream past the dirt purge jets and leaks across the tip gap contributing to the low pressure region downstream of the second dirt purge hole.

Tip Adiabatic Effectiveness Results. The dirt purge holes serve the functional purpose of expelling dirt from the blade that might otherwise block smaller film cooling holes. Any cooling from the dirt purge holes would be an added benefit. The cooling effects of the dirt purge geometry are presented as adiabatic effectiveness according to Equation 4-2. Figure 4-7 reports

the adiabatic effectiveness contours for a large tip gap case at four different blowing ratios from the dirt purge holes. The images show only the leading edge half of the blade because no cooling effects from the dirt purge holes occurs near the trailing edge. At the lowest blowing ratio, the dirt purge holes cool a strip of the blade surface. There is even cooling evident upstream of the first dirt purge hole. At such a low blowing ratio, it is unlikely that this upstream cooling is a result of flow impinging upon the shroud and returning to the tip. Furthermore, the upstream coolant is confined to the dirt purge cavity, which indicates that the cavity behaves much like the squealer geometry studied by Kwak and Han [2002a,b]. Circulating flow within the cavity draws coolant from the dirt purge towards the leading edge. When the blowing ratio is increased to 0.19%, the majority of the dirt purge flow does not appear to attach to the tip surface until it has cleared the dirt purge cavity. As a result, only a small path that is about the width of the dirt purge cavity experiences cooling levels above $\eta = 0.50$. As the blowing ratio increases to 0.29%, a larger area of the tip experiences cooling including areas upstream of the dirt purge cavity. At 0.38% there appears to be increased spreading, possibly due to impingement on the shroud. Of the four blowing ratios, the greatest effectiveness ($\eta = 0.94$) was present at the highest blowing ratio. The 0.29% blowing ratio had a maximum level of $\eta = 0.78$ inside the dirt purge cavity next to the second hole. With the 0.19% blowing ratio the maximum effectiveness of $\eta = 0.59$ was located where the coolant reattached outside of the dirt purge cavity. The maximum adiabatic effectiveness dropped to $\eta = 0.57$ for the 0.10% blowing ratio and was located inside the cavity next to the second dirt purge hole. Outside of the cavity, the maximum occurred at the point of reattached flow with $\eta = 0.50$. It is also interesting to note that, the lowest blowing ratio provided better cooling inside the dirt purge cavity than the 0.19% blowing ratio.

Figure 4-8 shows adiabatic effectiveness contours for the small tip gap at the same four blowing ratios as for the large tip gap. We notice a dramatic increase in adiabatic effectiveness with a smaller tip gap. The maximum effectiveness for the lowest blowing ratio was 0.86 while the 0.19%, 0.29%, and 0.38% blowing ratios reached $\eta = 1.0$. At the 0.19%, 0.29%, and 0.38% blowing ratios, a completely cooled region stretches from the pressure side of the tip to the suction side. That is, η is nearly equal to 1 throughout this region. The leading edge region is completely flooded with coolant as flow exiting the dirt purge holes impacts the shroud and then propagates outward in all directions. This flooding of the tip gap prevents hot leakage flows from

ever entering the tip region at the leading edge, so the dirt purge blowing serves as a significant blockage of tip leakage at the small tip gap.

In order to better quantify the amount of cooling the dirt purge holes provide, an average of the adiabatic effectiveness values are taken laterally along the blade. A MATLAB code written by Christophel [2003] divides the blade into thin slices as shown in Figure 4-9, and the average effectiveness is calculated over the area of each slice before being plotted along the X-direction. The width of a slice (ΔX) was 1.25% of the blade axial chord, but Figure 4-9 exaggerates the magnitude of ΔX for clarity. Figure 4-10 shows the laterally averaged adiabatic effectiveness plot for the large tip gap. The X-locations of the dirt purge holes are labeled with vertical dashed lines. The average effectiveness spikes up at the dirt purge holes because the areas of the dirt purge hole exits are factored into the average as having an effectiveness of 1.0. With the large tip gap, effectiveness increases with blowing ratio, especially near the dirt purge holes. The smallest increase in averaged effectiveness occurs when the blowing ratio is increased from 0.10% to 0.19%. As mentioned earlier, cooling levels within the dirt purge cavity are actually higher in the 0.10% case than in the 0.19% case. An explanation for the decreased cooling with increased blowing is offered a little later. For all cases, the cooling effects of the dirt purge holes diminish at a normalized x-location of $X/B_X = 0.6$.

Figure 4-11 shows the laterally averaged adiabatic effectiveness for the small tip gap. The peak average effectiveness for the 0.10% blowing ratio occurs at the same X-location as the second dirt purge hole. With the small tip gap, the averaged effectiveness increases drastically from the 0.10% to the 0.29% blowing case, but the trend does not continue. The averaged effectiveness levels for the 0.38% blowing ratio are not significantly larger than those at 0.29% blowing. Because tip temperatures can be no lower than the coolant temperature, there is an apparent limit to the amount of cooling that can be gained by increasing the coolant flow from the dirt purge holes. The coolant that floods the tip gap is eventually swept away with the tip leakage into the mainstream flow and does not remain in the tip gap past $X/B_X = 0.6$ to cool regions closer to the trailing edge. This is an important result for the gas turbine industry because the amount of air used to cool the turbine blades has an adverse effect on the overall engine efficiency. The small amount of cooling gained by increasing the blowing ratio beyond 0.29% may not be worth the detraction from engine performance.

All of the effectiveness measurements for dirt purge only cases are summarized in Figure

4-12. Effectiveness values are averaged over the entire area of the blade for each case and then plotted against blowing ratio for both tip gap sizes. This average includes the trailing edge area so that it may be compared later to other cases that include the entire blade. The trailing edge region was accounted into the average using effectiveness values of 0 because it is unaffected by blowing from the dirt purge holes. Overall the small tip gap shows higher effectiveness levels than the large tip gap for each blowing ratio. The small tip gap shows that average effectiveness increases with blowing ratio. The large tip gap case shows that the average effectiveness only slightly increases when the blowing ratio is increased from 0.10% to 0.19%. The reason for this is that at the lowest blowing ratio cooling is provided to the tip because the coolant is injected into the tip gap with a small amount of momentum so that it attaches to the tip surface immediately. At the highest blowing ratio the coolant is injected with so much momentum that it impacts the shroud and turned back to cool the tip surface. At the blowing ratios between these two extremes, the momentum of the injected coolant is high enough that it cannot initially attach to the tip surface yet low enough that it does not sufficiently impact the shroud to return to the tip. Some of this coolant reattaches to the tip surface further downstream while the rest is lost to the tip leakage flow.

Summary of Results. Originally intended to prevent dirt and dust particles from clogging smaller film cooling holes, the dirt purge holes heavily influence film-cooling near the leading edge of the tip gap region. Overall, the Cp distribution on the shroud shows lower pressures with a large tip especially above the dirt purge holes. At high blowing ratios large zones of low pressure occur around the entire leading edge. Contours of adiabatic effectiveness verify that these zones are not caused by tip leakage flow but are a result of coolant from the dirt purge holes. The dirt purge jets act as a blockage of mainstream leakage and flood the leading edge region at higher blowing ratios. Increased blowing resulted in higher adiabatic effectiveness levels for a large tip gap. While effects from the dirt purge holes are greater with a small tip gap, coolant blow-off to the mainstream limits the amount of film cooling gained by increased blowing ratio.

The adiabatic effectiveness results from this section suggest that the dirt purge holes may serve more than a functional purpose. Furthermore, the effectiveness of film cooling from the

dirt purge is drastically improved with a small tip gap as air from the dirt purge floods the tip gap and prevents the hot mainstream flow from leaking across the tip gap.

4.5 Microcircuit Case

This section presents the results from tests conducted with the combined blowing from microcircuit film cooling holes and the dirt purge holes. Static pressure measurements on the shroud are presented first, followed by adiabatic effectiveness measurements, and, finally, cooling effectiveness measurements on the tip. The static pressure readings on the shroud were made using the foam tip although blade material should be irrelevant for those measurements. Surface temperature measurements on a foam tip were used to calculate adiabatic effectiveness, and temperatures on an alumina tip were used to calculate cooling effectiveness. All measurements were made at four different blowing ratios: 0.5%, 1.0%, 1.5%, and 2.0% of the mass flow through one passage. As with the dirt purge only geometry, we tested tip gap heights at 0.54% and 1.63% of the blade span. These tip gap heights are referred to as the small and large tip gaps, respectively.

Shroud Pressure Distribution Results. Pressure measurements on the shroud with microcircuit and dirt purge blowing are reported here in terms of a dimensionless pressure coefficient, C_p, which is defined in Equation 4-1. Figure 4-13 shows the shroud pressure distributions for the baseline case and at four different blowing ratios with a large tip gap. The white regions signify large, positive C_p values that are outside the range of values on the colorbar. To allow comparison between blowing ratios, the range is not adjusted to accommodate the large C_p values. Instead, the maximum C_p value is labeled in two regions: high pressure regions caused by the dirt purge blowing and high pressure regions caused by microcircuit blowing.

The microcircuit blowing appears to have dramatic effects on the shroud pressure distribution with a large tip gap as compared with Figure 4-4 with only dirt purge blowing. Differences between the pressure distributions of the baseline case and the lowest blowing ratio are noticeable at the midchord. Here, the low pressure region indicating the *vena contracta* becomes less defined as higher pressures are present in the tip gap. At the 1.0% case, midchord

pressures continue to increase, and white regions of high pressure begin to form on the pressure side outside the tip gap. These high pressure regions are likely caused by microcircuit blowing impinging on the shroud. The microcircuit blowing disturbs the leakage flow entering the pressure side so that the separation bubble that causes the *vena contracta* is weakened. As a result, we might expect the tip leakage vortex to be affected since it is thought to be caused by the relative velocities of the mainstream flow and the tip leakage flow (Bindon, 1989). Indeed, higher pressures appear to be present in the region of the tip leakage vortex at the 1.0% blowing ratio. At higher blowing ratios of 1.5% and 2.0%, the contours of the tip leakage vortex become distorted, which hints strongly at a reduction in the tip leakage vortex. This is a significant result that supports assertions made by Prasad [1999] that pressure side blowing could diminish the tip leakage vortex. We also observe the formation of a high pressure region between the dirt purge jets, which is similar to the one that was observed in cases with only dirt purge blowing.

Figure 4-14 shows static pressure contours for the baseline case and for four blowing ratios with a small tip gap. Again, we see slightly increased pressures on the midchord and a diminished tip leakage vortex with higher blowing ratios. There are extremely low pressures forming around the high pressure region above the dirt purge holes. The high pressure zone characterizes dirt purge jets impinging on the shroud, and the low pressure regions indicate that this impinging flow is turned so that high velocities are present parallel to the shroud.

Tip Adiabatic Effectiveness Results. Surface temperature measurements on the foam tip with microcircuit film cooling and dirt purge blowing were converted to adiabatic effectiveness using Equation 4-2. Tip adiabatic effectiveness distributions at four blowing ratios with a large tip gap are presented in Figure 4-15. The black arrows mark the locations of the microcircuit exits, and the exits are numbered in Figure 4-15a according to the scheme introduced in Chapter 3.

The large tip case shows increased cooling with increased blowing ratio. A large portion of the leading edge shows low effectiveness as coolant from exit 2 is swept toward the pressure side. Exit 1 does not appear to add much cooling to the leading edge for a 0.5% blowing ratio. Effectiveness levels in this region steadily increase with increased blowing until effectiveness levels between 0.9 and 1.0 are present at the 2.0% case. Tests with only dirt purge blowing

showed that parts of the leading edge saw no cooling, but the combination of the microcircuit and dirt purge cools the entire leading edge region.

The lowest blowing ratio has distinguished stripes of cooling associated with the microcircuit exits. These stripes are slightly offset from the microcircuit exits indicating that the injected coolant is swept towards the trailing edge before entering the tip gap. At higher blowing ratios there appears to be more spreading at the midchord. For the 1.0% case, exits 11 through 15 cause spots of effectiveness around 0.5 to occur along the pressure side. With increased blowing, these spots disappear suggesting that either coolant separates from the tip or is blown off into the mainstream.

At the trailing edge, there is a large uncooled portion of the tip between exits 15 and 16. The coolant from exit 16 does not appear to hold to any trend with blowing ratio. There may be increased spreading at higher blowing ratios, but effectiveness levels fluctuate between each case.

Microcircuit effectiveness levels increase dramatically with a smaller tip gap as shown in Figure 4-16. On the whole, cooling levels on the tip with a small tip gap are not affected by blowing ratio as they are on the large tip gap. The leading edge region is almost entirely cooled for every blowing ratio as the dirt purge blowing floods the tip gap. Effectiveness levels approach 1.0 in this region. The midchord region also shows improved cooling over the large tip case. As the blowing ratio increases, the cooling from exits 14 and 15 appears to decrease. As with the large tip gap, decreased cooling at the midchord at higher blowing ratios could be the result of coolant entering the blade passage rather than flowing over the tip. There appears to be an uncooled region between exits 15 and 16, except for the 0.5% blowing case. At 0.5% blowing, the coolant from exit 15 extends further towards the trailing edge than it does at any other case. Much like the large tip gap cases, there does not appear to be any trend in the cooling from exit 16.

Figure 4-17 shows laterally averaged adiabatic effectiveness for the large tip gap plotted against normalized axial chord position. The vertical, dashed lines indicate the positions of the dirt purge holes, which are factored into the average as having a value of $\eta = 1.0$. Overall, there is increased cooling with increased blowing. However, from $X/B_X = 0.7$ to 1.0, cooling levels for the 1.5% case are higher than the 2.0% case. The greatest increase in cooling occurs between the 0.5% case and the 1.0% case. The small tip lateral averages, shown in Figure 4-18, have higher

effectiveness levels and little variation between blowing ratios than the large tip cases. Around the dirt purge holes, effectiveness levels for all blowing ratios remain between 0.8 and 1.0 with higher blowing ratios having higher effectiveness levels. From $X/B_X = 0.6$ to the trailing edge of the blade, the lowest blowing ratio has the highest laterally averaged effectiveness. The increased cooling at the trailing edge is a result of the increased spreading of coolant from exit 15.

While microcircuit cooling can be observed at the midchord and trailing edge, film cooling at the leading edge appears to be dominated by the dirt purge holes. It is not yet clear how much cooling, if any, is offered by microcircuit exits in the leading edge region. Hohlfeld [2003] predicts that the 0.19% and 0.29% blowing ratios in the dirt purge only case pass the same mass flow through the dirt purge holes as the 1.0% and 1.5% blowing ratios in the combined microcircuit and dirt purge case. Based on this calculation, we can observe the impact the microcircuit has on cooling in the leading edge region. Figure 4-19 compares laterally averaged adiabatic effectiveness between dirt purge only cases and cases with combined dirt purge and microcircuit blowing with a large tip gap. For both 0.19% and 0.29% blowing ratios, we can see that adiabatic effectiveness levels are increased by the presence of microcircuit blowing. With 0.19% blowing from the dirt purge holes, peak lateral average effectiveness levels increase from 0.34 to 0.77. At 0.29% dirt purge blowing, peak levels rise from 0.67 to 0.83. On average, the presence of the microcircuit increases lateral averages on the leading edge ($X/B_X = 0$ to 0.6) by 0.34 for the 0.19% case and by 0.31 for the 0.29% case.

Figure 4-20 shows laterally averaged effectiveness with dirt purge blowing compared to that with blowing from the dirt purge and microcircuit with a small tip gap. At the 0.19% blowing ratio, the microcircuit improves cooling for a only small portion of the leading edge from $X/B_X = 0$ to $X/B_X = 0.03$. Lateral averages for the rest of the leading edge up to the first dirt purge hole are the same with and without the microcircuit. The peak lateral average of adiabatic effectiveness actually drops from 0.97 to 0.96 when microcircuit blowing is present. Overall, the microcircuit causes an average increase of 0.14 in lateral averages on the leading edge. At the 0.29% blowing ratio, this average drops to a 0.05 increase. It appears that the microcircuit does not increase laterally averaged effectiveness levels immediately around the dirt purge holes as maximum laterally averaged effectiveness values are 0.98 for cases with microcircuit blowing and 1.00 for cases without.

Figure 4-21 shows adiabatic effectiveness averaged over the entire blade tip for all geometries. Effectiveness levels with a small tip gap vary little with blowing ratio, while on a large tip gap effectiveness levels experience greater increases at low blowing ratios than at high blowing ratios. For all blowing ratios, area averaged adiabatic effectiveness was higher for a small tip gap than with a large tip gap. This may, in part, be a result of enhanced film cooling from the dirt purge holes with a small tip gap. The average effectiveness levels with blowing from the dirt purge only are more than twice as large with a small tip gap as with a large tip gap (except at the highest blowing ratio). The adiabatic effectiveness results show the effects of film cooling from the microcircuit and dirt purge exits. In the following, cooling effectiveness results will account for internal convection as well as film cooling.

Tip Cooling Effectiveness Results. All heat transfer results presented thus far are from tests performed on an adiabatic blade surface, so that internal convection from microcircuit passages can be considered negligible. The results that will now be presented are from surface temperature measurements that were made on an alumina blade tip. The Biot number of alumina is matched to that of an actual turbine blade, so that internal convection effects of the microcircuit can be observed in addition to film cooling effects. Cooling effectiveness is presented here with tip contours, laterally averaged cooling effectiveness plots, and area averaged cooling effectiveness plots.

Figure 4-22 shows cooling effectiveness results for a large tip gap. The differences between the adiabatic effectiveness and cooling effectiveness contour patterns indicate that tip temperatures are being affected by internal convection from the microcircuit. The contours are more spread out than the streaky contours of the adiabatic effectiveness contours shown in Figure 4-15. Also, instead of the being swept towards the trailing edge, the cooled regions at the midchord are closer to the microcircuit exits. With the large tip gap, there is a noticeable improvement in effectiveness with increased blowing at the leading edge. This tends to be the case in the midchord region as well, with one exception. At 0.5% blowing, there are spots of higher cooling effectiveness near exits 8 thru 15 that appear to drop off slightly when the blowing ratio is increased to 1.0%. This drop off is limited to the pressure side of the blade as cooling increases near the suction side. At 1.5% blowing, the coolest areas on the midchord occur in the center of the blade as the lower areas of effectiveness occur along the pressure and

suction sides. These areas continue to spread across the midchord at 2.0% blowing, and cooling effectiveness levels continue to increase. A steady increase in cooling can be observed at the leading edge when blowing is increased, while there appears to be a reduction in cooling at the trailing edge.

The cooling effectiveness contours for a small tip gap are shown in Figure 4-23. A noticeable increase in cooling effectiveness along the entire blade occurs between blowing ratios of 0.5% and 1.0%. However, the contours at 1.0%, 1.5%, and 2.0% appear to be very similar both in pattern and magnitude. The greatest difference in these three cases occurs at the trailing edge. The typically hot region between exits 15 and 16 has abnormally high effectiveness levels at the 1.5% blowing ratio, but these drop off at the 2.0% case. Inside the trailing edge, a thin air passage extends from the midchord microcircuit passage to exit 16. By design, this passage intended to gain some internal cooling at the trailing edge, but there is not sufficient evidence to show that this significantly reduces tip temperatures. The region from exit 15 to 16 is virtually uncooled for all cases.

Lateral averages of cooling effectiveness were calculated in the same way as the adiabatic effectiveness cases. Figure 4-24 shows laterally averaged cooling effectiveness plotted against normalized axial chord for the large tip gap case. The vertical dashed lines label the axial locations of the dirt purge holes which are factored into the average as having values of $\phi = 1.0$. As was noticeable in the contour plots, there is steady increase in cooling effectiveness levels as blowing ratio increases except at the trailing edge. At axial locations from $X/B_X = 0.8$ to 1.0, there are smaller variations between blowing ratios that do not follow any clear trend.

Figure 4-25 presents the plot of laterally averaged cooling effectiveness for a small tip gap. The lowest blowing ratio provides less cooling over the majority of the blade than the higher blowing ratios that have little variation between them in cooling effectiveness. As in the adiabatic effectiveness results, the small tip gap case has higher effectiveness levels at the leading edge than the large tip case. Yet, at the midchord region, average cooling effectiveness levels are similar for large and small tip gap cases. It is possible that the film cooling from the dirt purge holes plays a significant role in cooling the leading edge region, and we have seen from adiabatic cases that film cooling from the dirt purge varies greatly with tip gap size. On the other hand, the cooling effectiveness at the midchord may be dominated by internal cooling which we would not expect to vary as greatly with tip gap size. It is more likely that there is a

trade-off between film cooling and convective cooling. With increased blowing ratio, higher internal heat transfer coefficients stabilize effectiveness levels as film cooling is lost to blow-off. It was earlier noted that Figure 4-22 showed the highest midchord cooling effectiveness levels shift from the pressure side at 0.5% cooling to the blade center at 1.5% cooling. This further illustrates that film cooling lost to blow-off at higher blowing ratios is recovered by increased internal cooling. There may be a more optimal microcircuit geometry that provides high internal heat transfer coefficients while maintaining lower exit velocities, so that coolant is not ejected into the mainstream flow.

Area averages of cooling effectiveness for each case are presented in Figure 4-26. At every blowing ratio average effectiveness is higher for a small tip gap. The large tip gap shows a steady increase in effectiveness with blowing ratio, while the small tip gap shows a large increase in effectiveness between 0.5% and 1.0% and smaller increases afterwards.

Summary of Results. It has been shown that blowing from the microcircuit has favorable cooling and aerodynamic implications. Distributions of static pressure coefficient on the shroud show that the tip leakage vortex is diminished. This supports findings by Prasad [1999] that pressure side injection could reduce the tip leakage vortex and the aerodynamic losses associated with it. The pressure side injection also provides coolant across the tip gap. The large tip gap has higher adiabatic effectiveness with higher blowing ratios, but effectiveness does not vary greatly with blowing ratio at the small tip gap. The static pressure contours indicate that the coolant exiting the microcircuit impacts the shroud with a small tip gap. Some coolant leaks across the tip gap and some of it blows off into the mainstream flow giving way to similar effectiveness levels between blowing ratios.

The dirt purge holes offer significant film cooling to the leading edge, but it has been shown that laterally averaged effectiveness levels are improved with microcircuit blowing. The microcircuit offers increased adiabatic effectiveness levels and a greater coverage of film cooling over the tip. While the microcircuit delivers coolant to the leading edge and midchord regions in all test cases, there is a region at the trailing edge between exits 15 and 16 that is not cooled by internal convection or film cooling. Computational predictions of adiabatic effectiveness from Hohlfeld [2003] also indicate that this region is uncooled. The experimental work shows that, at the small tip gap and lowest blowing ratio, coolant from exit 15 is spread toward the trailing edge

cutting the uncooled region in half. It may be beneficial to alter the microcircuit design so that more coolant is distributed to exits on the leading edge and less to the exits near the trailing edge.

Results from this research will contribute to calculating the temperature profile of the blade volume. Experimental cooling effectiveness and adiabatic effectiveness values were used to calculate the ratio of internal and external heat transfer coefficients. The next section explains this calculation and gives the results.

4.6 Heat Transfer Analysis

Chapter 1 outlines a method of numerically analyzing heat transfer in the microcircuit and deriving temperatures at any point in the blade volume. To carry out such an analysis, proper boundary conditions are required on the blade surfaces. The effectiveness results from this research will contribute to the calculation of a distribution of heat transfer coefficients on the external tip surface, h_g, and the internal surfaces of the microcircuit air passages, h_c. Adiabatic and cooling effectiveness data can be used to arrive at a ratio of heat transfer coefficients, h_{gc}. Further testing presented in Christophel [2003] will provide the data needed for a complete distribution of h_g and h_c.

Calculating Heat Transfer Coefficient Ratio, h_{gc}. Adiabatic wall temperature, T_{aw}, and metal temperature, T_m, can be backed out of Equations 4-2 and 4-3, respectively, using a common mainstream temperature value, T_∞, and coolant temperature at the inlet to the microcircuit, T_c. Therefore, T_{aw} was calculated from Equation 4-2 using

$$T_{aw} = T_\infty - \eta\left(T_\infty - T_c\right) \qquad (4\text{-}5)$$

where T_∞ is the mainstream temperature from the alumina tip tests (cooling effectiveness), and T_c is the coolant temperature from the alumina tip tests. Future tests by Christophel [2003] will provide an average between the coolant inlet and exit temperatures, but for these calculations T_c is the measured temperature of the coolant inlet. T_m can be backed out from Equation 4-3 in the same manner as T_{aw}, but, because mainstream and coolant temperatures from the alumina tests are used, the original tip temperature data can be used straightaway. T_{aw} and T_m can now be used to calculate h_{gc}.

As explained in Chapter 1, the adiabatic wall temperature represents the gas temperature distribution on a tip with film cooling from the microcircuit. The metal temperature is the tip surface temperature and can be substituted into Equation 1-7 for T_{s1}. With this substitution, the external to internal heat transfer coefficient ratio, h_{gc}, can be backed out of Equation 1-7 with

$$h_{gc} = \left(\frac{T_{aw} - T_c}{T_{aw} - T_m} \right) - 1 . \qquad (4\text{-}6)$$

The thermal conductivity of the alumina material is high enough that the Biot number was dropped from Equation 4-6.

Heat Transfer Coefficient Ratio Results. The heat transfer coefficient ratio was calculated for each test case using the method outlined in the previous subsection. The h_{gc} values are included in Appendix G and will not be discussed until tests are completed by Christophel [2003]. The nature of Equation 4-6 is such that, when metal temperatures approach adiabatic wall temperatures, the denominator becomes very small and h_{gc} approaches infinity. If T_{aw} is only slightly larger than T_m, then h_{gc} is a large positive number. If T_{aw} is slightly smaller than T_m, than h_{gc} is a large negative number.

Heat is always transferred to the turbine blade causing heat transfer coefficients to be positive at all times. As was mentioned earlier, the results from this analysis are based on coolant inlet temperatures instead of localized coolant temperatures within the microcircuit. These calculations do not account for heat added to the coolant as it travels through the microcircuit. While the heat transfer coefficient ratio results are not complete, the adiabatic effectiveness and cooling effectiveness were measured on a tip with a microcircuit geometry. The conclusions from these tests are presented in the next chapter.

Table 4-1 Summary of Engine and Tunnel Flows

Case	**Engine Flows** $\%\frac{\dot{m}_c}{m_e}$	**Wind Tunnel Flows** $\%\frac{\dot{m}_c}{\dot{m}_e}$
Microcircuit with Highest Blowing	3.58%	2.00%
Microcircuit with High Blowing	2.69%	1.50%
Microcircuit with Low Blowing	1.79%	1.00%
Microcircuit with Lowest Blowing	0.90%	0.50%
Dirt Purge with Highest Blowing	0.68%	0.38%
Dirt Purge with High Blowing	0.52%	0.29%
Dirt Purge with Low Blowing	0.34%	0.19%
Dirt Purge with Low Blowing	0.18%	0.10%

Table 4-2 Experimental Test Matrix

Geometry	Shroud Pressure Distribution Measurements	Tip Temperature Distribution Measurements
Flat Blade (Baseline)	**Large Tip Gap (1.63% Span)** No Blowing	
	Small Tip Gap (0.54% Span) No Blowing	
Dirt Purge Holes	**Large Tip Gap** 0.10% Blowing 0.19% Blowing 0.29% Blowing 0.38% Blowing	**Large Tip Gap** 0.10% Blowing 0.19% Blowing 0.29% Blowing 0.38% Blowing
	Small Tip Gap 0.10% Blowing 0.19% Blowing 0.29% Blowing 0.38% Blowing	**Small Tip Gap** 0.10% Blowing 0.19% Blowing 0.29% Blowing 0.38% Blowing
Dirt Purge Holes with Microcircuit: Adiabatic Case (Foam Material)	**Large Tip Gap** 0.5% Blowing 1.0% Blowing 1.5% Blowing 2.0% Blowing	**Large Tip Gap** 0.5% Blowing 1.0% Blowing 1.5% Blowing 2.0% Blowing
	Small Tip Gap 0.5% Blowing 1.0% Blowing 1.5% Blowing 2.0% Blowing	**Small Tip Gap** 0.5% Blowing 1.0% Blowing 1.5% Blowing 2.0% Blowing
Dirt Purge Holes with Microcircuit: Overall Cooling (Alumina Material)		**Large Tip Gap** 0.5% Blowing 1.0% Blowing 1.5% Blowing 2.0% Blowing
		Small Tip Gap 0.5% Blowing 1.0% Blowing 1.5% Blowing 2.0% Blowing

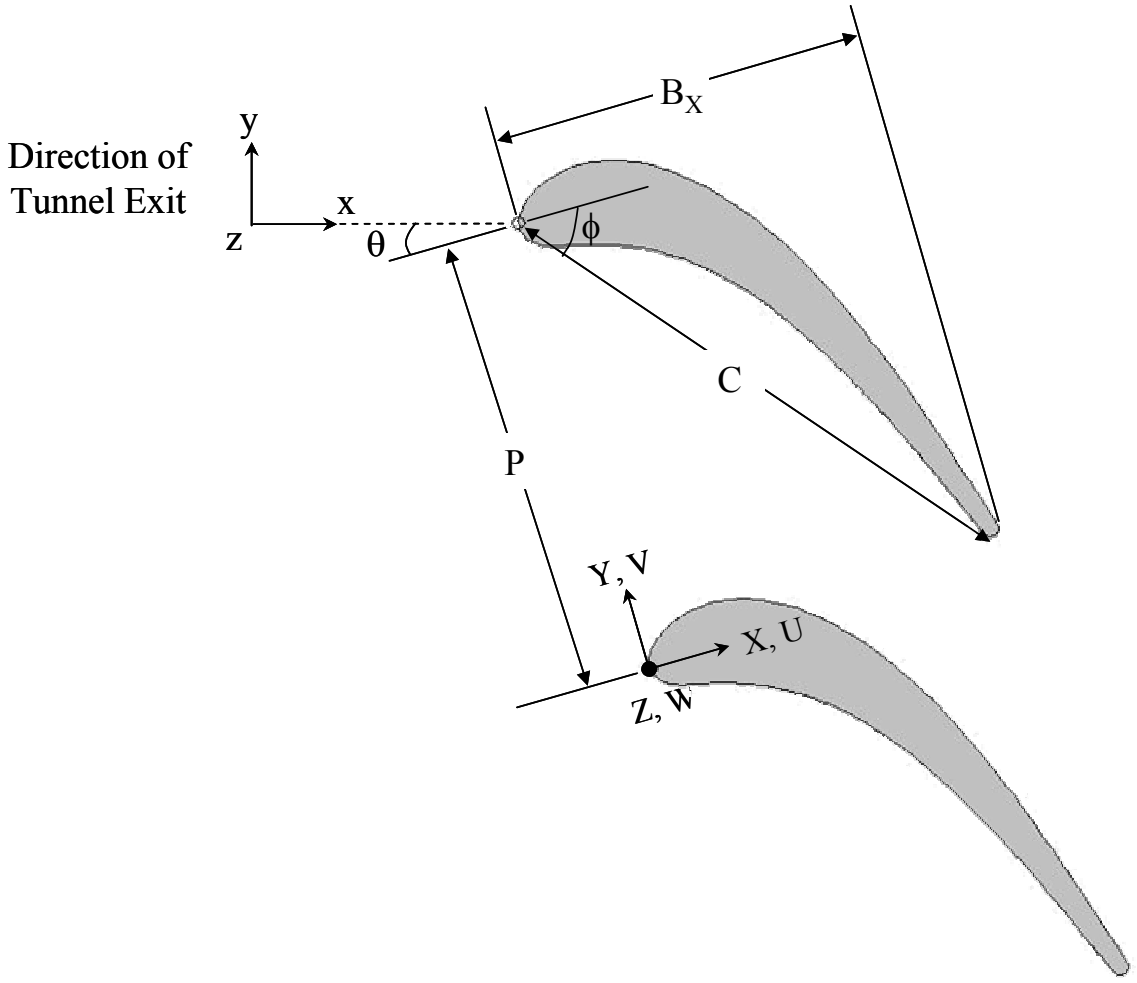

Figure 4-1 Geometric terminology for a turbine blade.

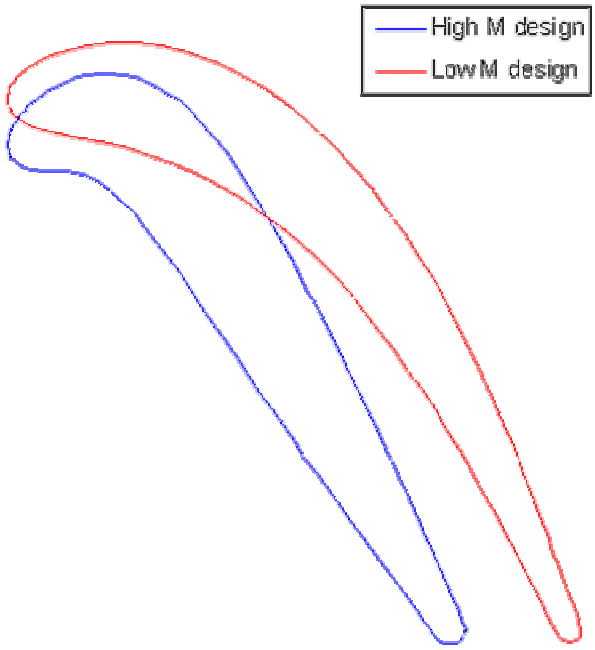

Figure 4-2 Two different designs for a turbine blade tip cross-section with the high-speed (engine) blade shown in blue and the low-speed (experimental) blade shown in red (Praisner, 2002).

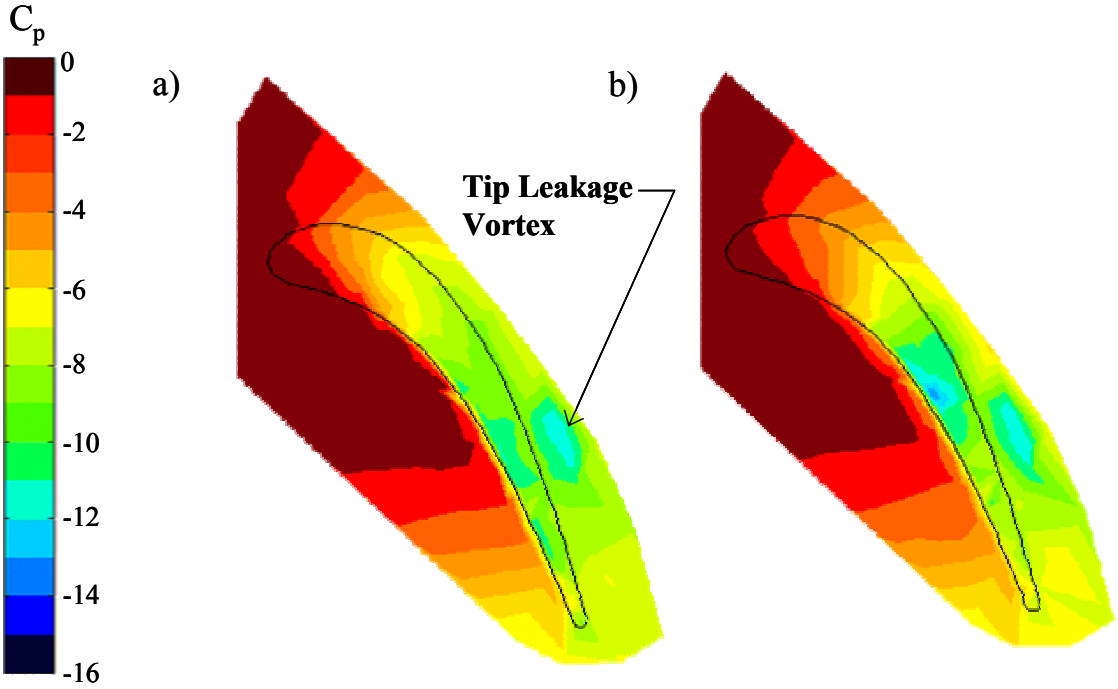

Figure 4-3 Shroud pressure distributions with a flat blade for a) a small tip gap and b) a large tip gap.

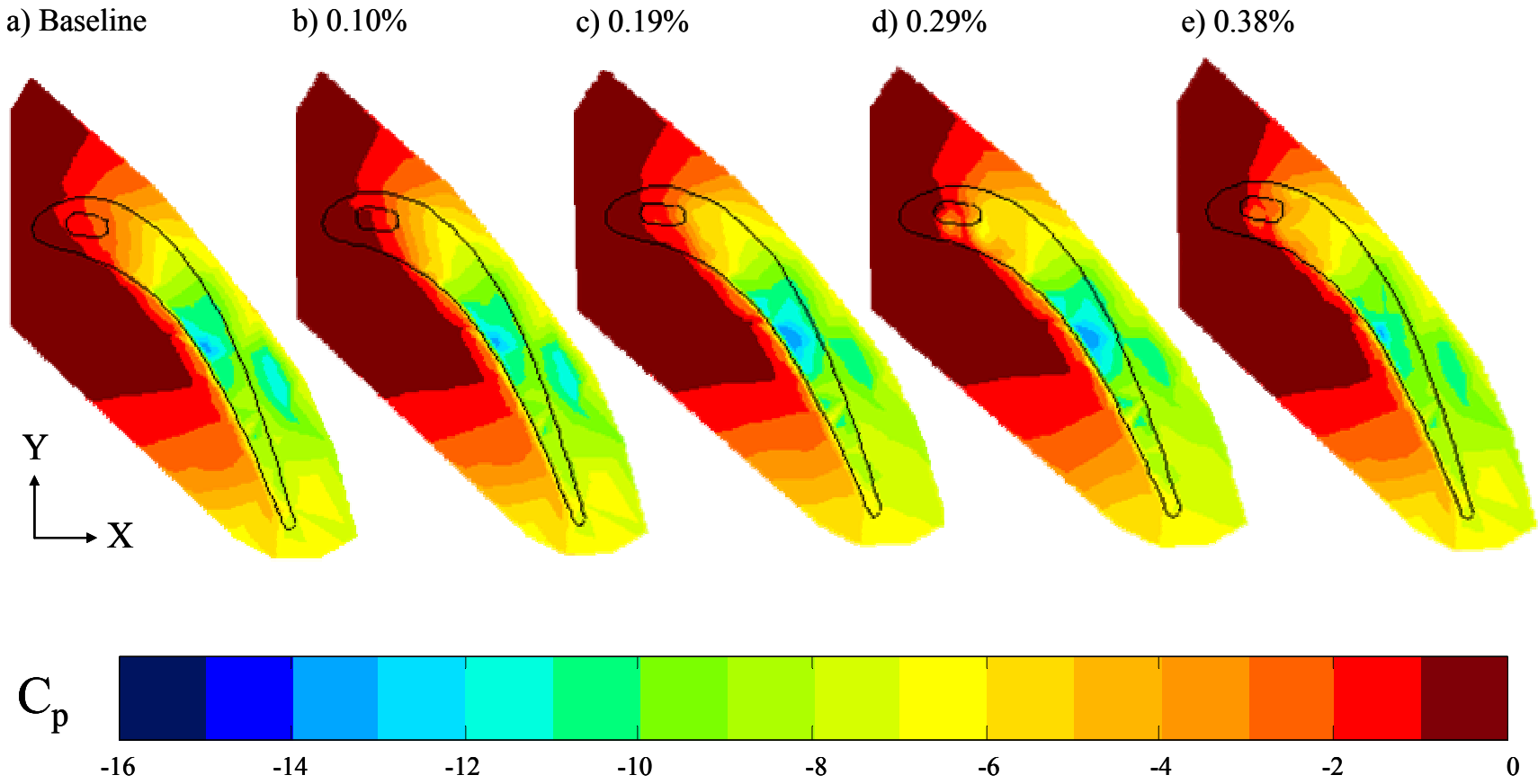

Figure 4-4 Shroud pressure distribution contours for a large tip gap at a) the baseline (flat tip) case, and at dirt purge blowing ratios of b) 0.10%, c) 0.19%, d) 0.29%, and e) 0.38%.

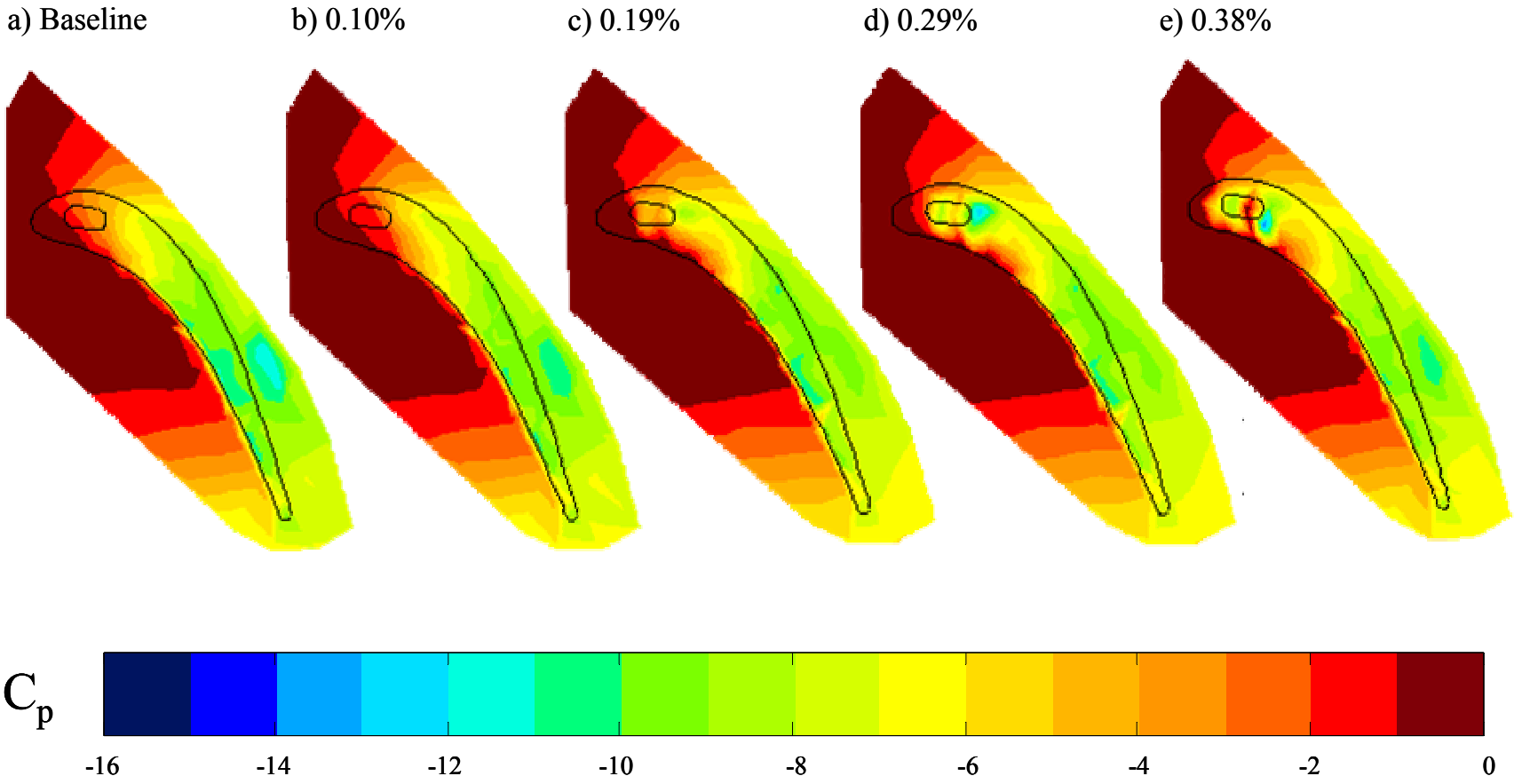

Figure 4-5 Shroud pressure distribution contours for a small tip gap at a) the baseline (flat tip) case and at dirt purge blowing ratios of b) 0.10%, c) 0.19%, d) 0.29%, and e) 0.38%.

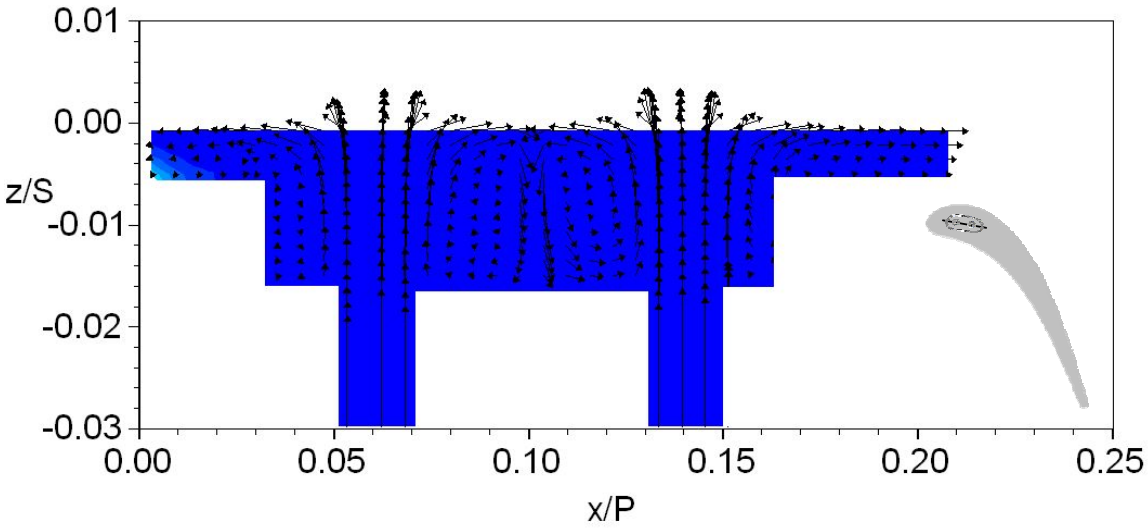

Figure 4-6 Cross section of the dirt purge cavity showing velocity vectors of coolant flows for a small tip gap with 0.29% blowing (Hohlfeld, 2003). The black line on the gray blade shape indicates the section plane location.

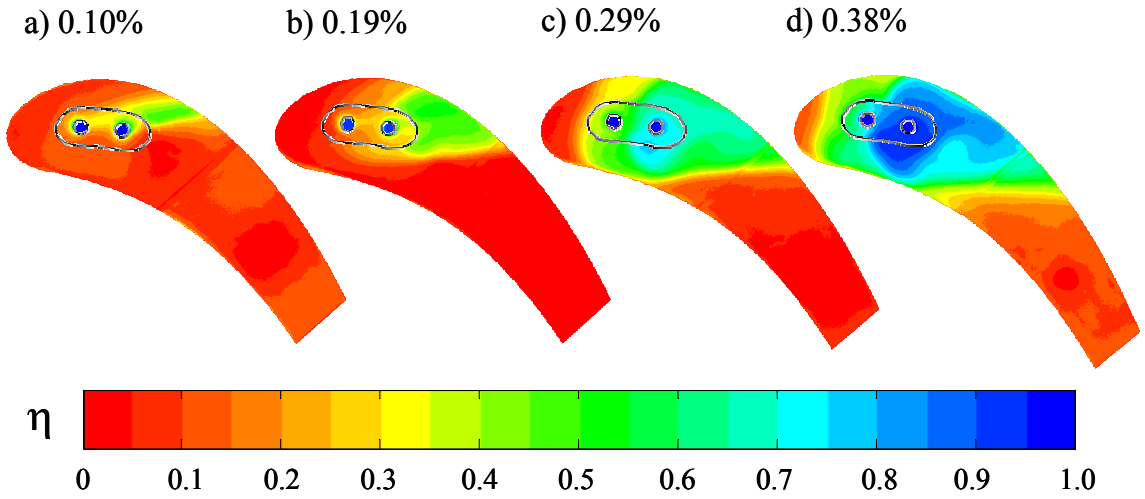

Figure 4-7 Large tip gap adiabatic effectiveness contours with dirt purge hole blowing ratios of a) 0.10%, b) 0.19%, c) 0.29%, and d) 0.38%.

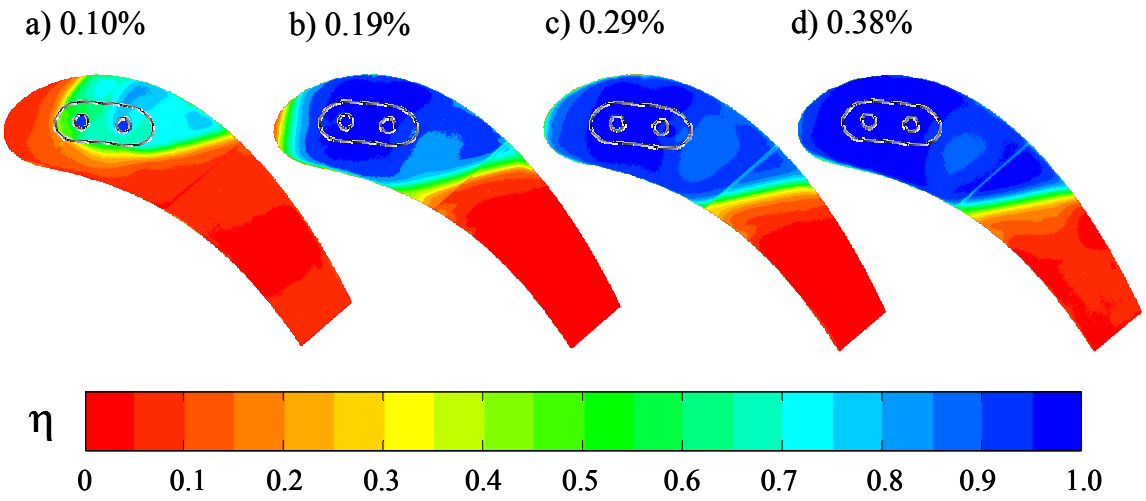

Figure 4-8 Small tip gap adiabatic effectiveness contours with dirt purge hole blowing ratios of a) 0.10%, b) 0.19%, c) 0.29%, and d) 0.38%.

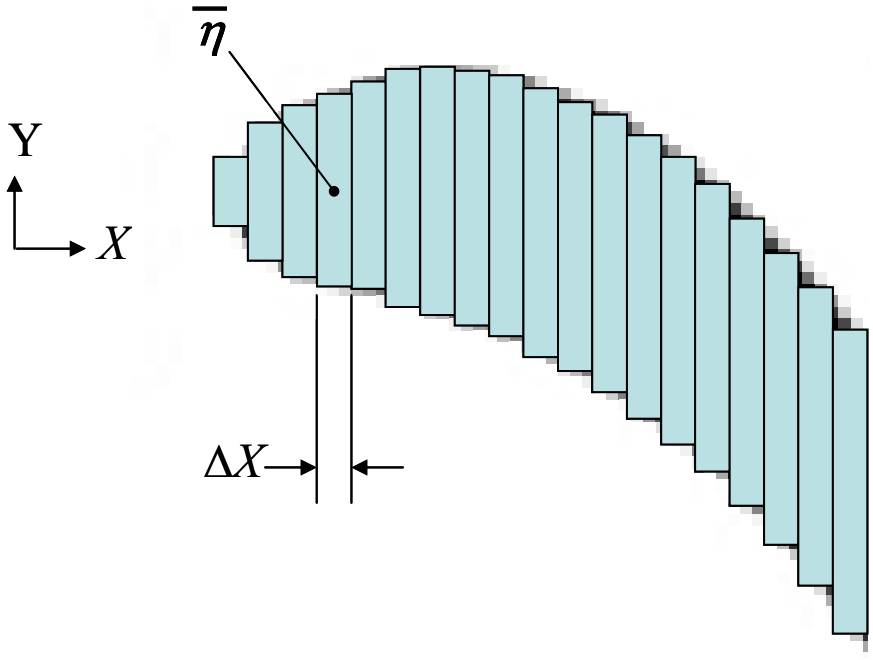

Figure 4-9 Scheme for lateral averaging of effectiveness values. A MATLAB code sliced the effectiveness data into thin areas normal to the flow and plotted the average effectiveness of each area against the X-direction.

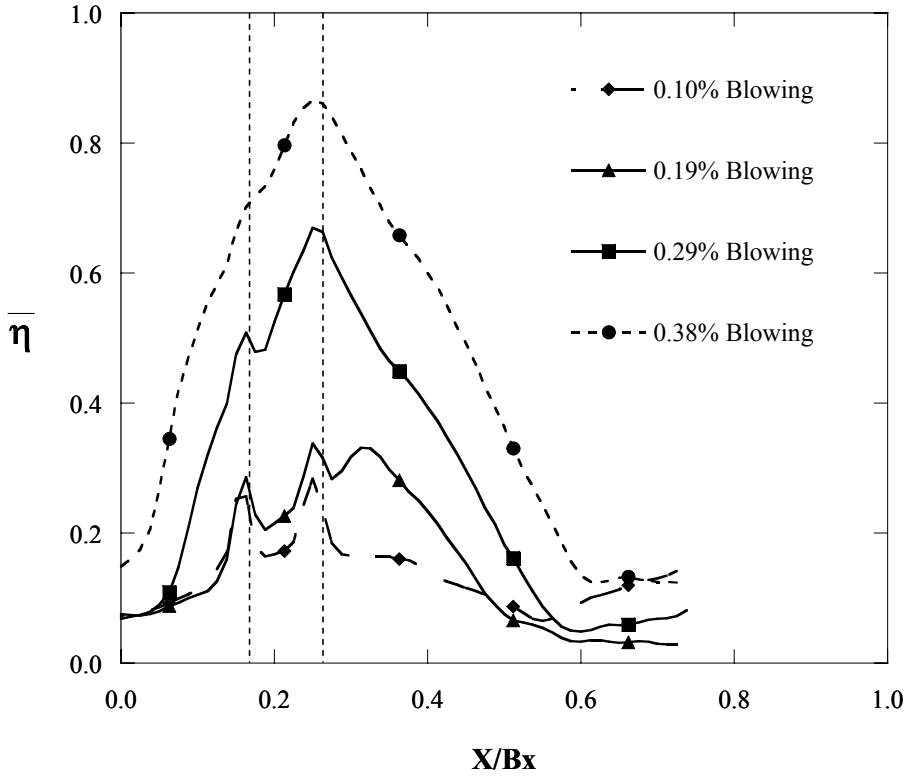

Figure 4-10 Laterally averaged adiabatic effectiveness at four dirt purge hole blowing ratios with a large tip gap plotted along the X-direction normalized by the axial chord length. The vertical dashed lines indicate the locations of the dirt purge holes.

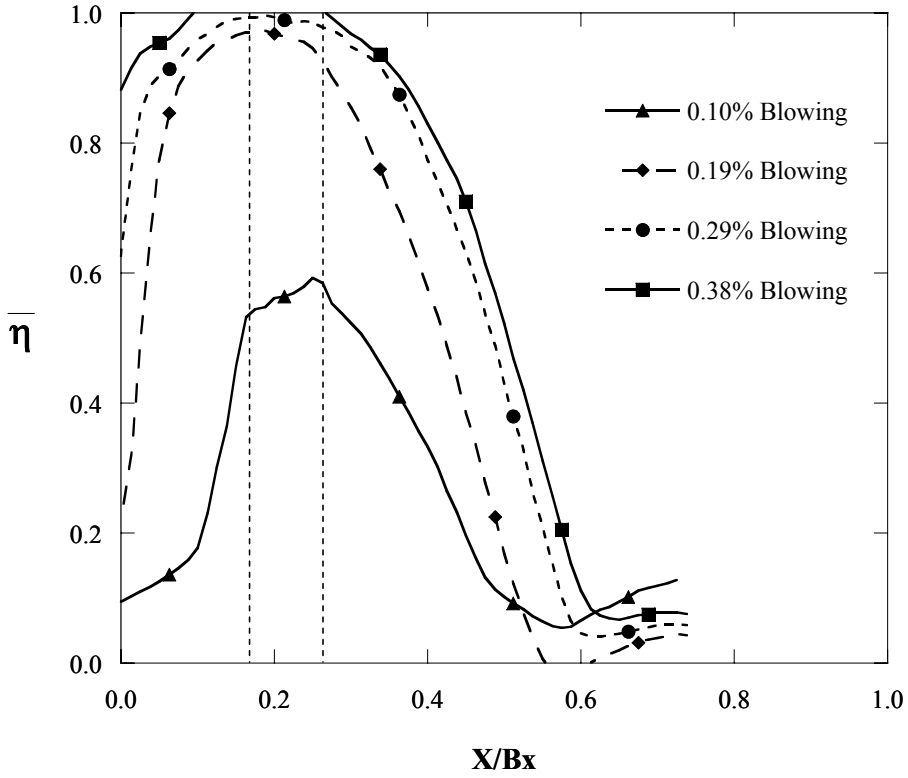

Figure 4-11 Laterally averaged adiabatic effectiveness at four dirt purge hole blowing ratios with a small tip gap plotted along the X-direction normalized by the axial chord length. The vertical dashed lines indicate the locations of the dirt purge holes.

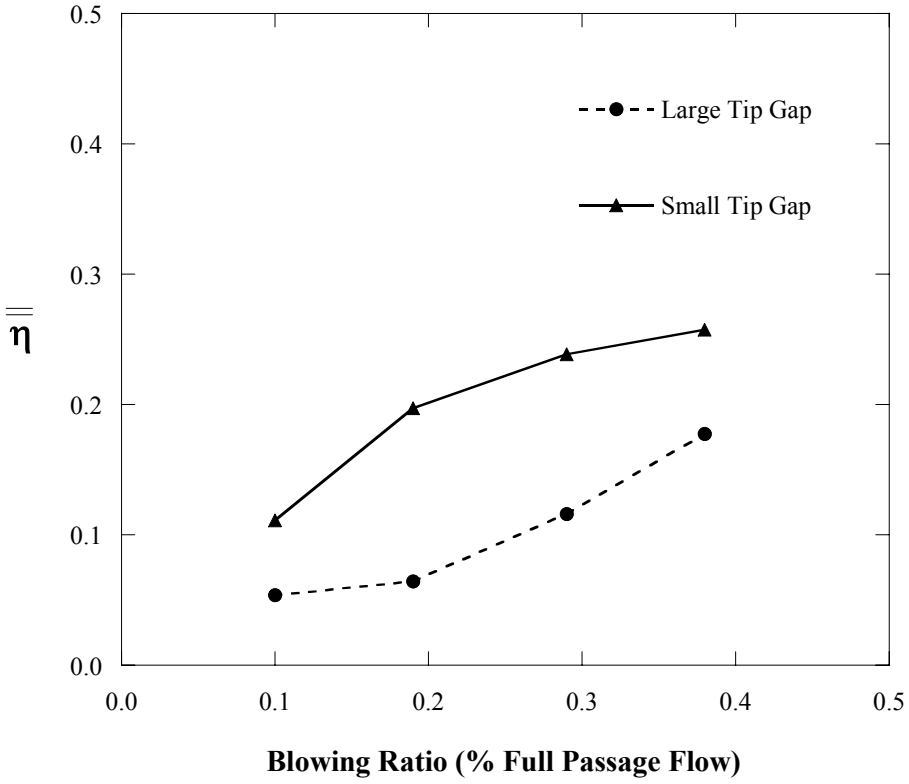

Figure 4-12 Adiabatic effectiveness averaged over the entire tip plotted against blowing ratio for a large and a small tip gap with blowing from the dirt purge only.

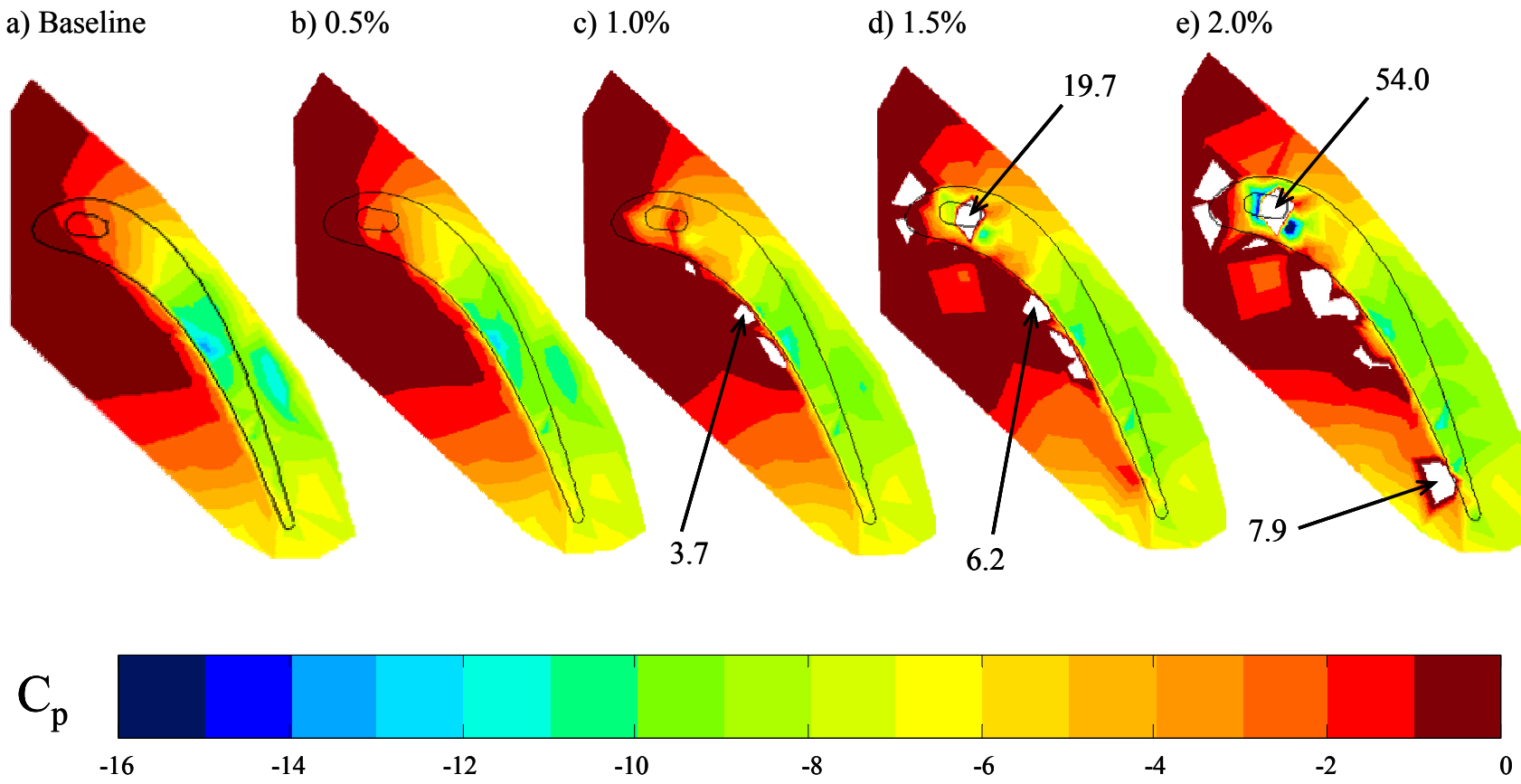

Figure 4-13 Shroud pressure distribution contours for a large tip gap at a) the baseline (flat tip) case, and at microcircuit blowing ratios of b) 0.5%, c) 1.0%, d) 1.5%, and e) 2.0%.

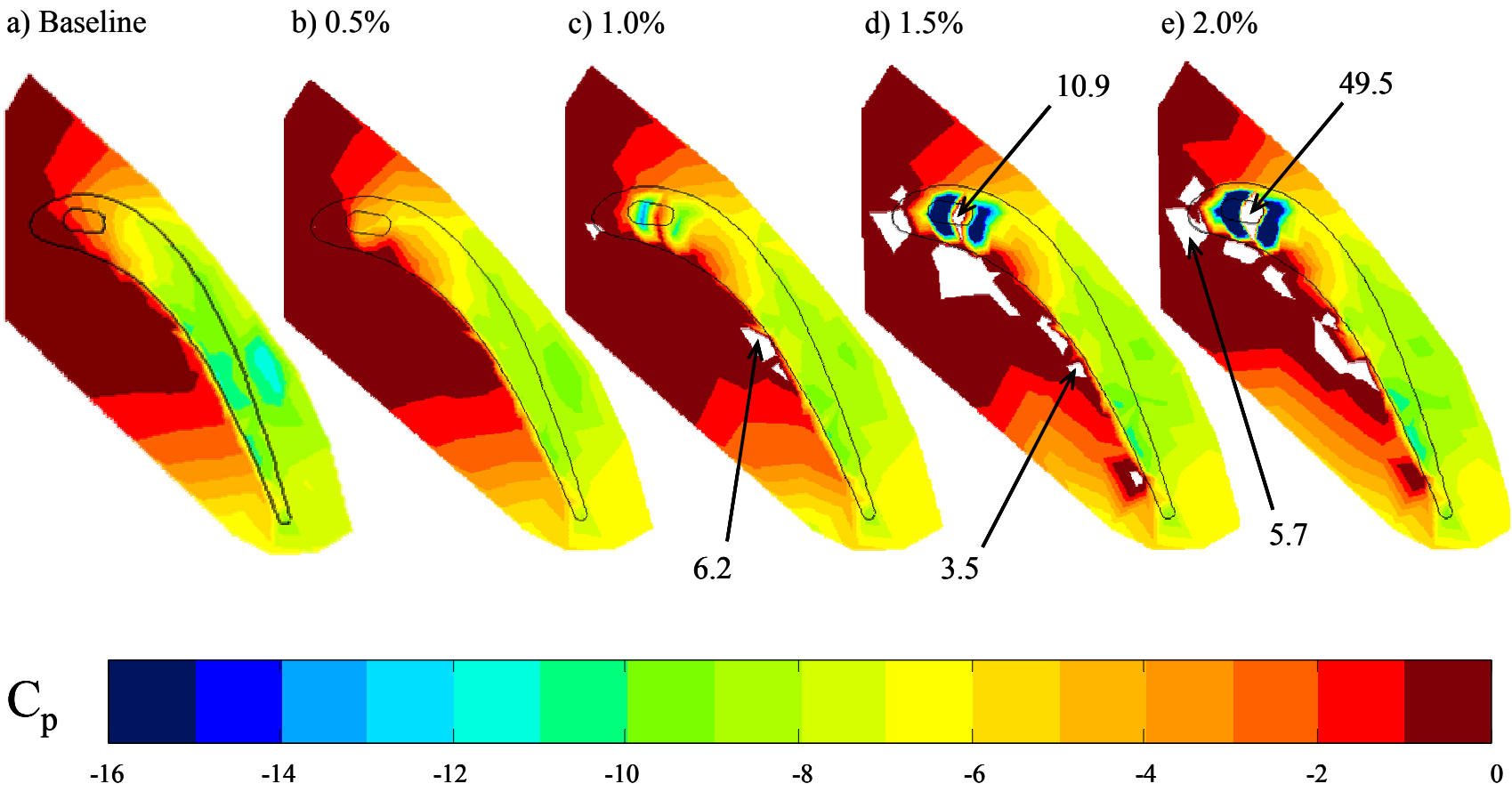

Figure 4-14 Shroud pressure distribution contours for a small tip gap at a) the baseline (flat tip) case, and at microcircuit blowing ratios of b) 0.5%, c) 1.0%, d) 1.5%, and e) 2.0%.

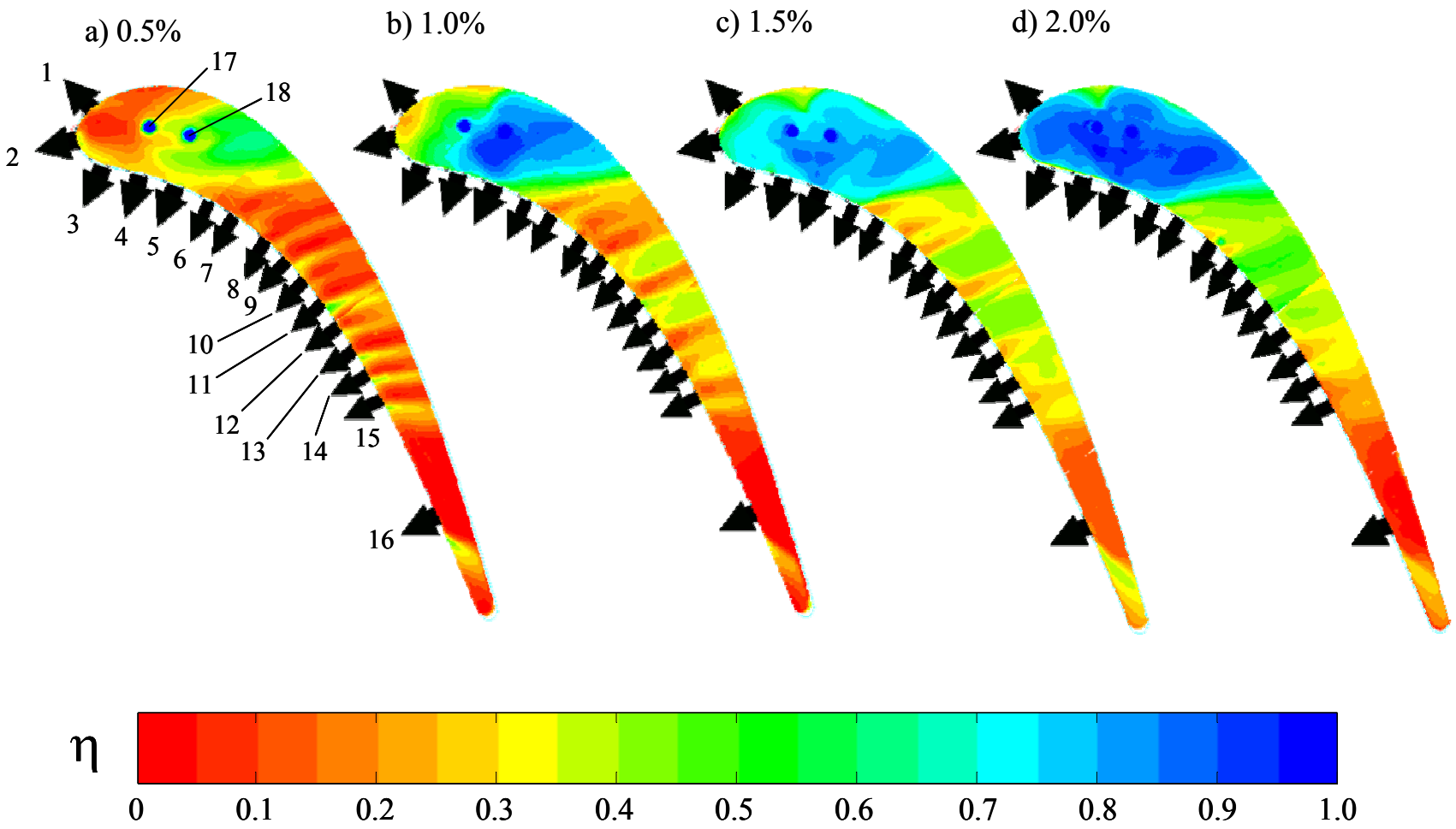

Figure 4-15 Tip adiabatic effectiveness contours for a large tip gap at microcircuit blowing ratios of a) 0.5%, b) 1.0%, c) 1.5%, and d) 2.0%. The black arrows label the locations of the microcircuit exits on the pressure side of the blade. The arrows in the 0.5% blowing case are numbered according to the scheme for the microcircuit and dirt purge exits that was laid out in Chapter 3.

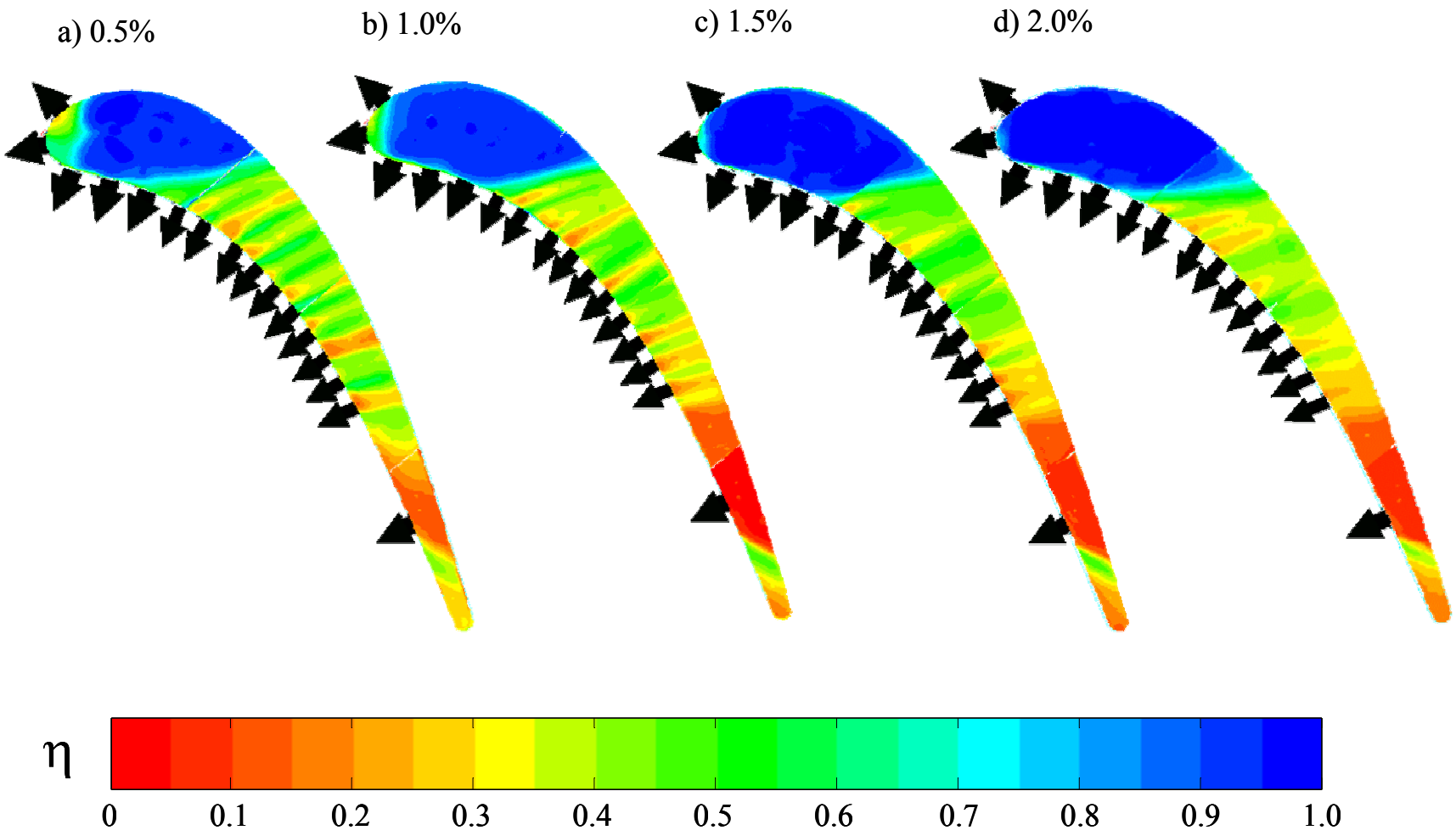

Figure 4-16 Tip adiabatic effectiveness contours for a small tip gap at microcircuit blowing ratios of a) 0.5%, b) 1.0%, c) 1.5%, and d) 2.0%.

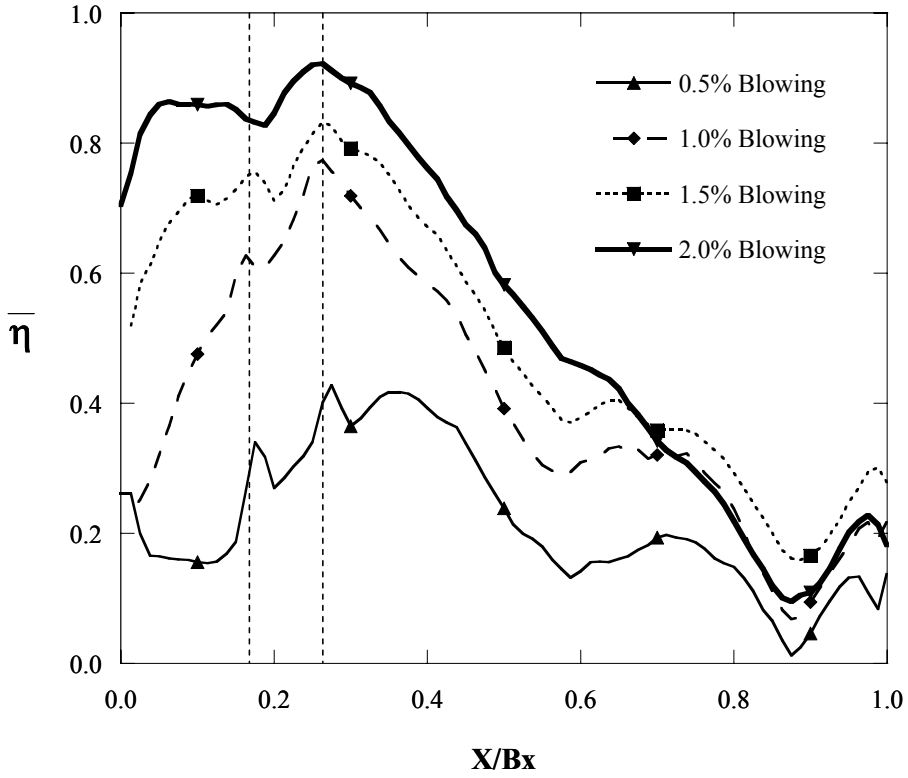

Figure 4-17 Laterally averaged adiabatic effectiveness at four microcircuit blowing ratios with a large tip gap plotted along the X-direction normalized by the axial chord length. The vertical dashed lines indicate the locations of the dirt purge holes.

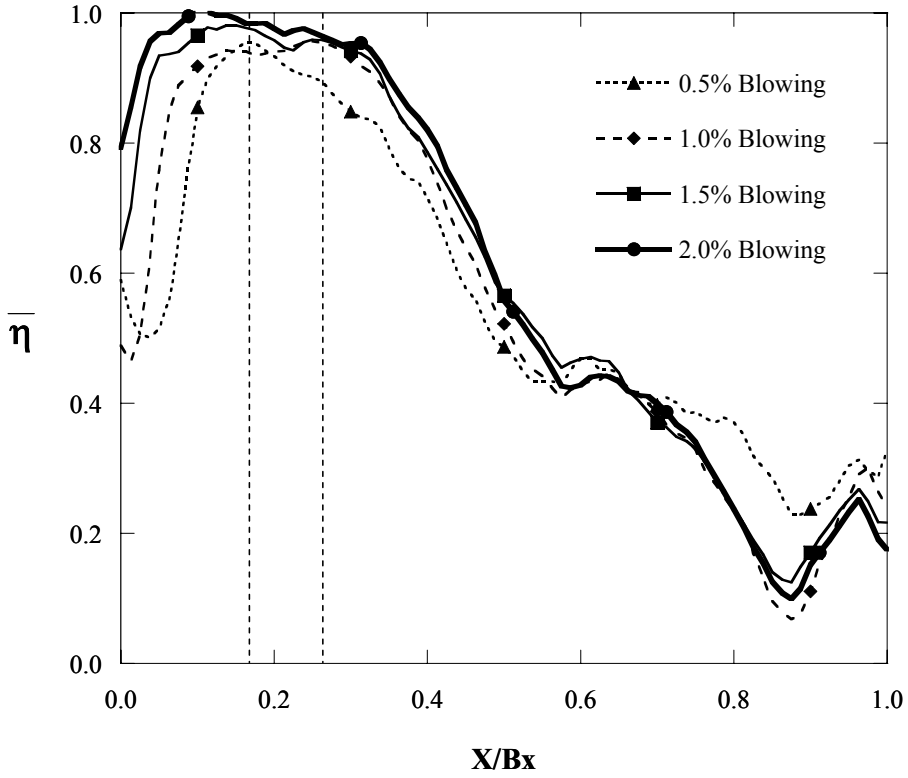

Figure 4-18 Laterally averaged adiabatic effectiveness at four microcircuit blowing ratios with a small tip gap plotted along the X-direction normalized by the axial chord length.

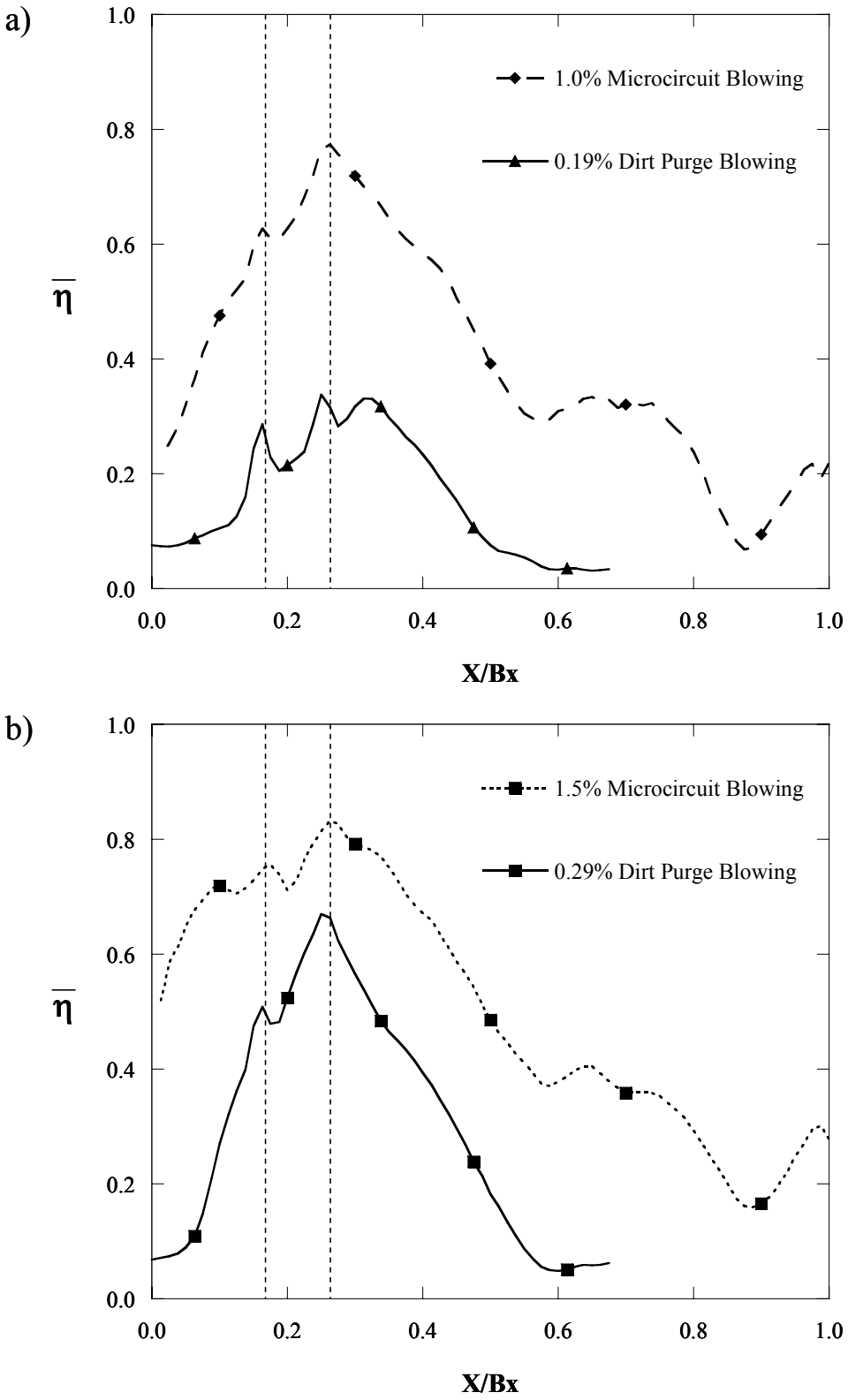

Figure 4-19 Laterally averaged adiabatic effectiveness with a large tip gap comparing a) 1.0% microcircuit with dirt purge blowing to 0.19% dirt purge only blowing and b) 1.5% microcircuit with dirt purge blowing to 0.29% dirt purge only blowing.

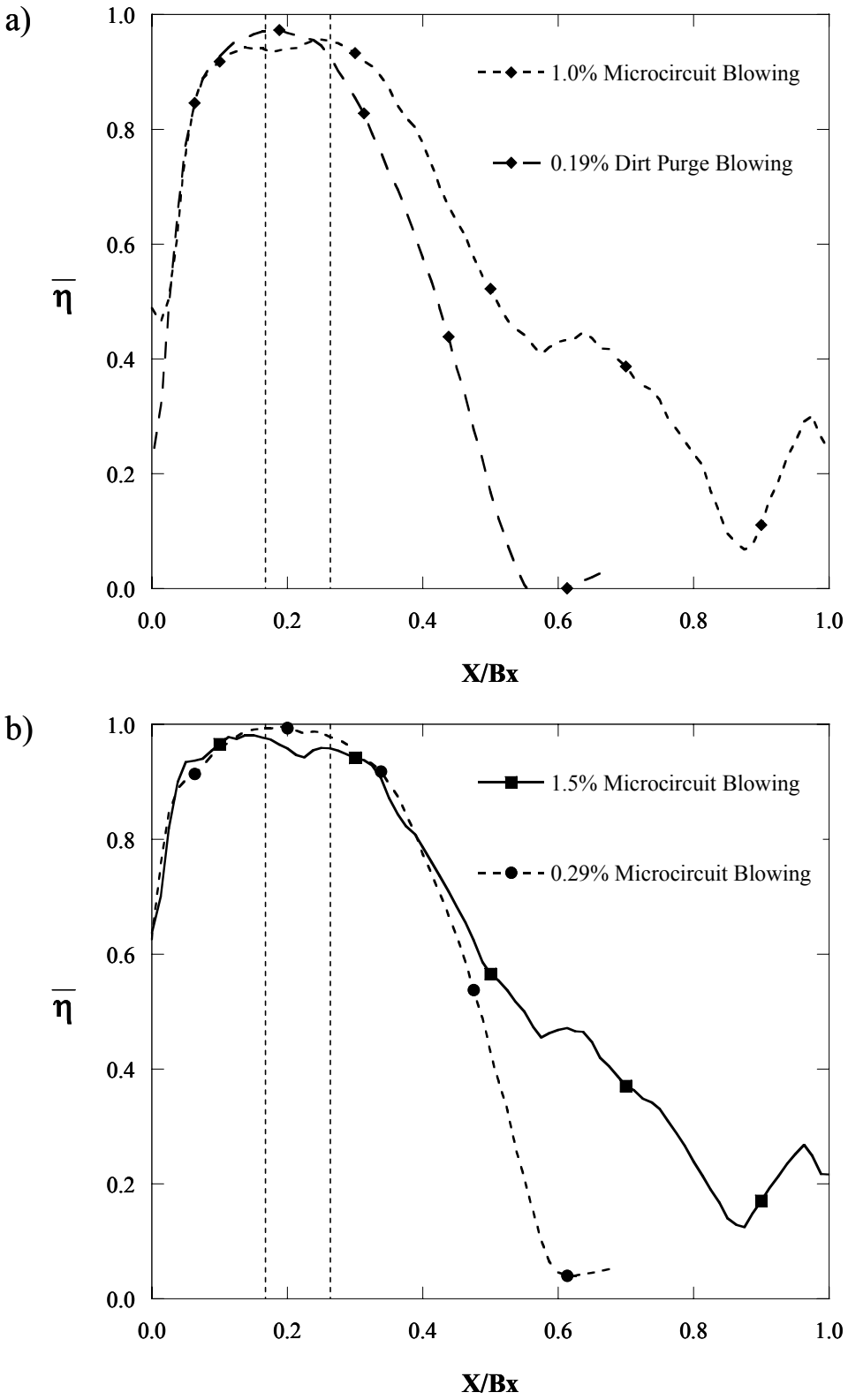

Figure 4-20 Laterally averaged adiabatic effectiveness with a small tip gap comparing a) 1.0% microcircuit with dirt purge blowing to 0.19% dirt purge only blowing and b) 1.5% microcircuit with dirt purge blowing to 0.29% dirt purge only blowing.

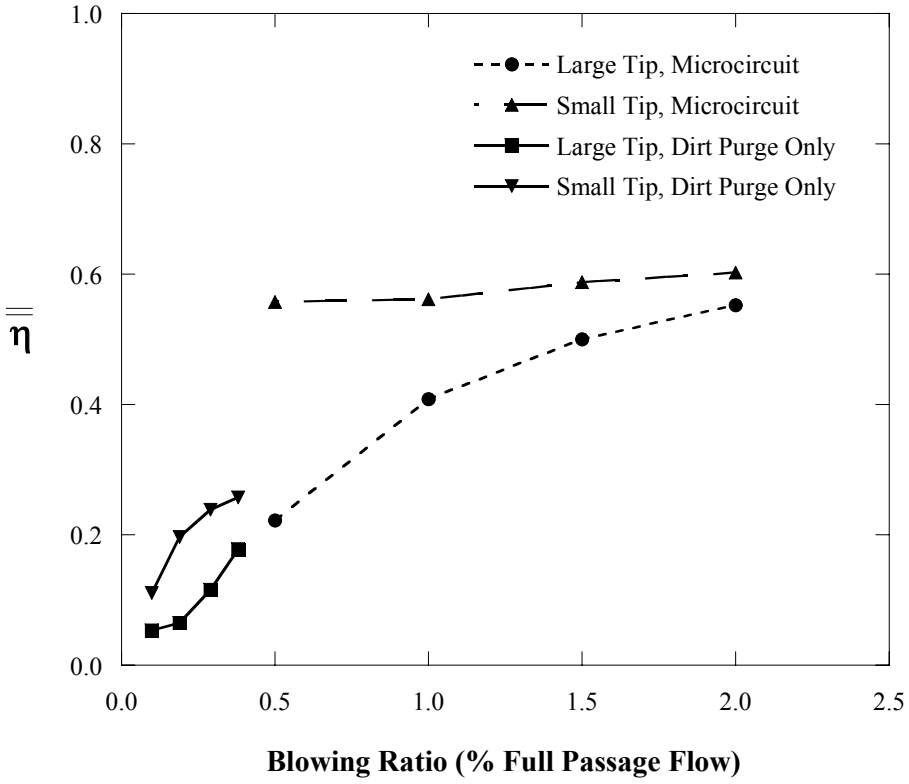

Figure 4-21 Adiabatic effectiveness averaged over the entire tip for all cases with dirt purge blowing only and with combined dirt purge and microcircuit blowing.

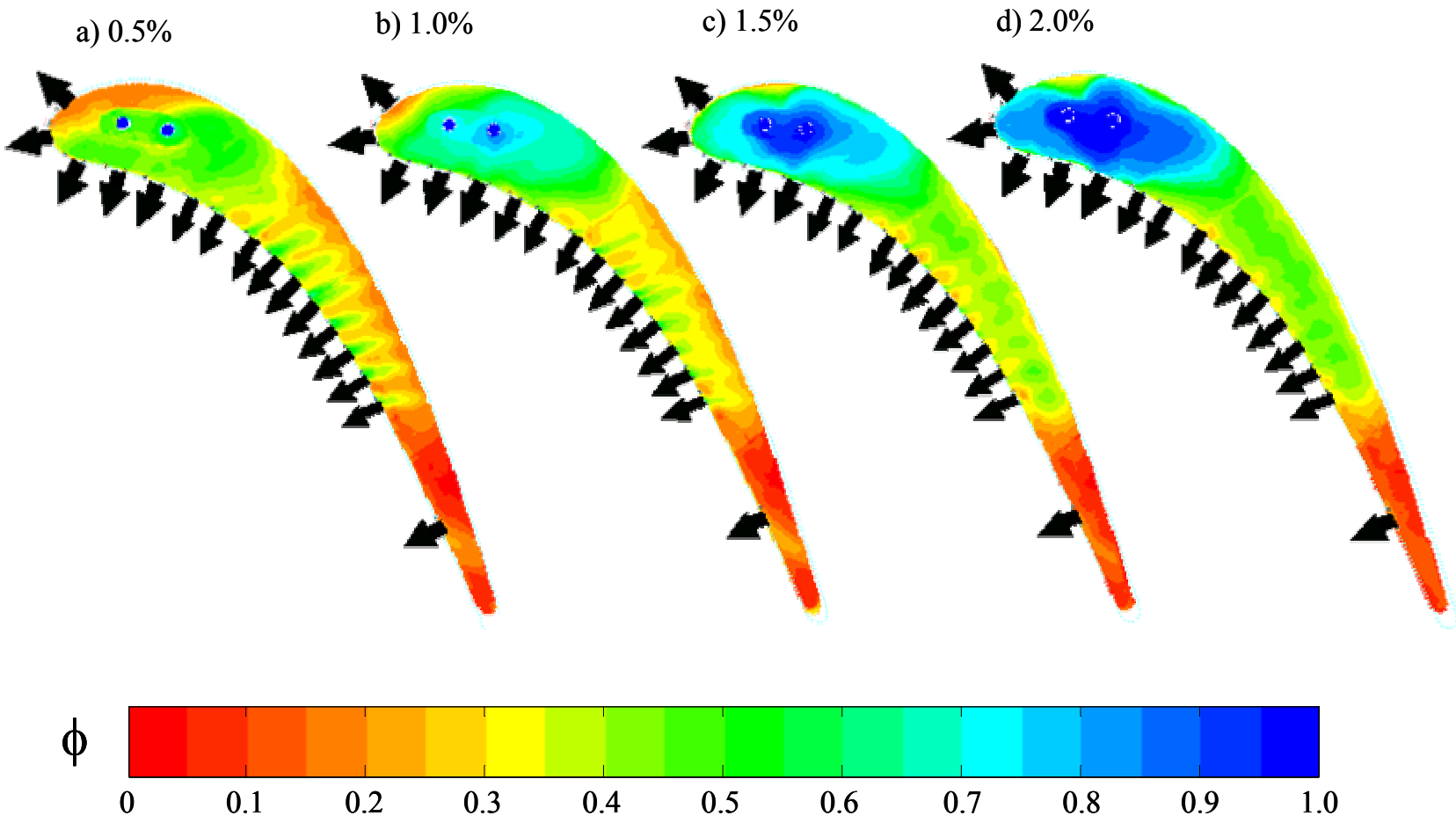

Figure 4-22 Tip cooling effectiveness contours for a large tip gap at microcircuit blowing ratios of a) 0.5%, b) 1.0%, c) 1.5%, and d) 2.0%.

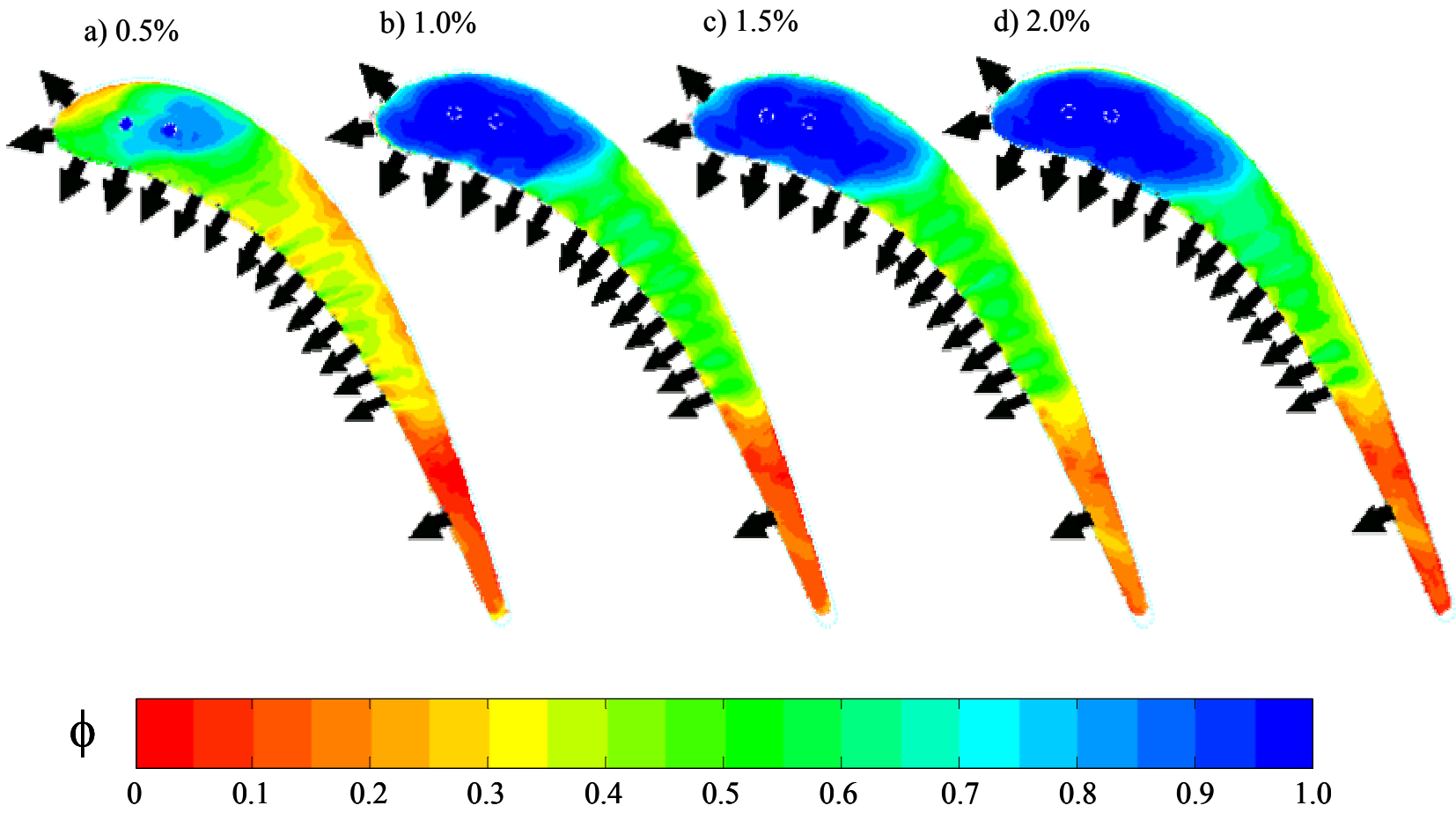

Figure 4-23 Tip cooling effectiveness contours for a small tip gap at microcircuit blowing ratios of a) 0.5%, b) 1.0%, c) 1.5%, and d) 2.0%.

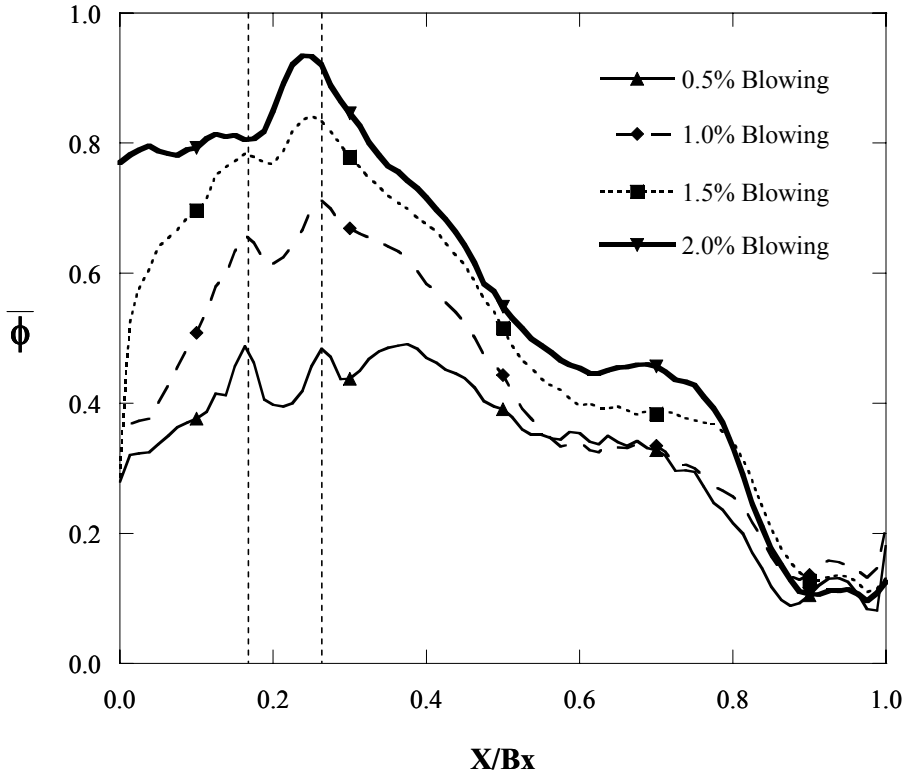

Figure 4-24 Laterally averaged cooling effectiveness for large tip gap at four microcircuit blowing ratios.

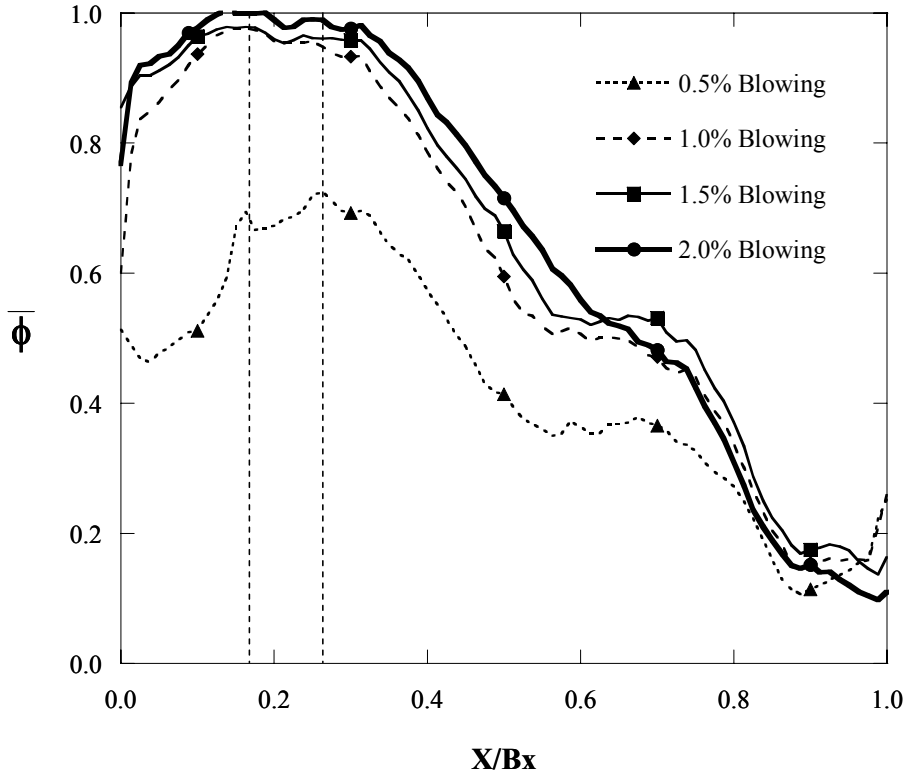

Figure 4-25 Laterally averaged cooling effectiveness for a small tip gap at four microcircuit blowing ratios.

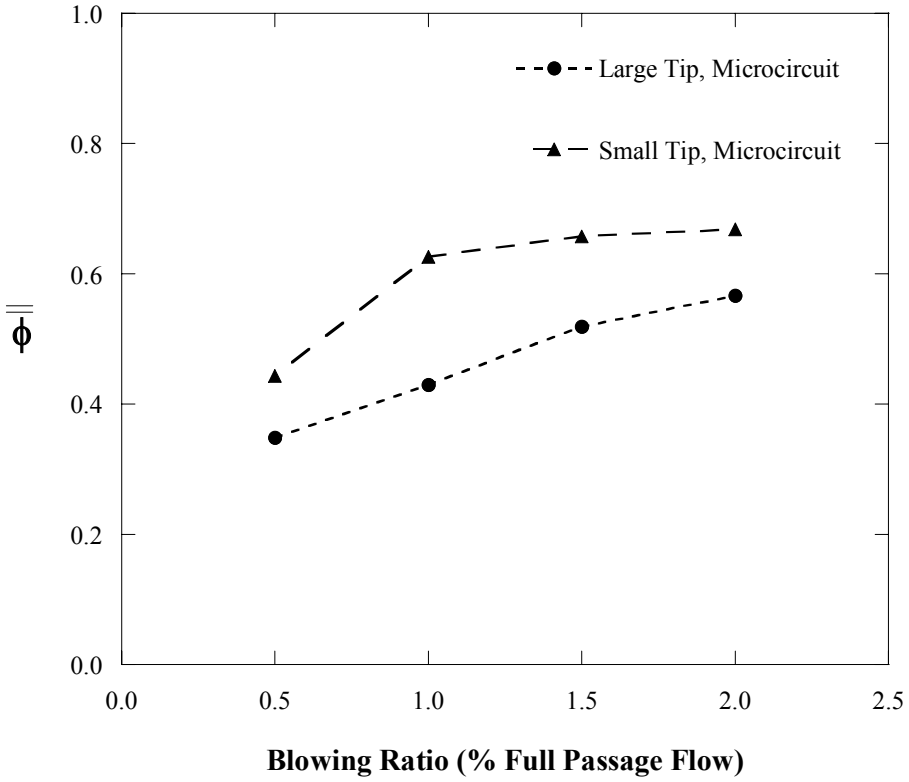

Figure 4-26 Area averaged cooling effectiveness plotted against blowing ratio for two tip gap sizes.

Chapter 5: Conclusions

This thesis reviews an extensive experimental study of a microcircuit design for the tip of a turbine blade. Previous work concerning flows and heat transfer in the tip region were reviewed in Chapter 2. There was a shortage of literature on heat transfer with blowing at the tip, and no literature exists on an experimental study of a microcircuit design. Chapter 3 outlined the facilities and methodologies of this particular experimental study, which was carried out in a low speed wind tunnel on large scale tip geometries. Chapter 4 presented results from flowfield and heat transfer studies on the tip region of the different geometries. These included a flat tip with no blowing, a tip with blowing from dirt purge holes, and a tip with blowing from dirt purge holes and microcircuit film-cooling holes. Static pressure coeffiecients on the shroud were presented for all geometries, and film-cooling studies gave adiabatic effectiveness values for the dirt purge only and dirt purge with microcircuit cases. Additional studies on an alumina tip revealed convective cooling effects of the microcircuit internal passages. In this final chapter, the first section draws conclusions for these results, and the following section offers recommendations for future testing.

5.1 Overview of Results

Tests were carried out on three geometries, the first of which was the case of a blade with a flat tip. This case served as a baseline to be compared to the other tip geometries. The static pressure distributions measured on the shroud revealed certain flow phenomena that are observed in open literature. Particularly, the presence of a low pressure region at the midchord area of the tip gap was observed. This region indicated a leakage of mainstream flow that increased with the size of the tip gap. A tip leakage vortex was also observed through a region of low pressure on the shroud off of the suction side of the blade.

Blowing from the dirt purge holes had major effects on flow and film cooling in the leading edge region. Shroud static pressure contours showed high gradients as jets of air from the dirt purge holes impacted the shroud. A region of high pressure could be

observed above the dirt purge holes as the jets were turned by the shroud and stagnate against each other. This stagnating air was also observed in computational results by Hohlfeld [2003]. When compared to the flat tip case, the effects of the dirt purge blowing were more prevalent with a small tip gap than with a large tip gap. This held true for the film cooling results as well. Adiabatic effectiveness contours suggest that, while blowing ratio was a factor, film cooling from dirt purge blowing is largely dependent on tip gap size. For the small tip gap case (1.63% of the span), coolant flooded the leading edge of the blade and blocked the hotter mainstream flow from entering the tip gap. With increasing blowing ratio, adiabatic effectiveness averaged over the area of the blades increased. However, the contours with a large tip gap (0.54% of the span) showed that coolant detached from the dirt purge cavity surface when the blowing ratio increased which is also observed in computational predictions by Hohlfeld [2003]. Overall, these results suggest that dirt purge holes can provide significant tip cooling in addition to serving the functional purpose of expelling dirt from the blade.

Although dirt purge blowing significantly cooled the leading edge, other regions of the blade remained uncooled. The addition of blowing from the microcircuit had significant effects on the entire tip region, particularly the midchord. In regard to the flowfield, this blowing seemed to block midchord leakage and diminish the formation of the tip leakage vortex as shown in static pressure distributions on the shroud. Trends pointed to higher adiabatic effectiveness with the small tip gap than with the large tip gap. The adiabatic effectiveness levels increased with higher blowing ratios on the large tip gap. However, there was little variation between coolant flows with the small tip.

Comparisons of laterally averaged adiabatic effectiveness indicated that blowing from the microcircuit in conjunction with blowing from the dirt purge holes improves film cooling for the large tip gap. The microcircuit delivered coolant to a majority of the tip surface, but there remained an area near the trailing edge that appeared untouched by coolant injection. The cooling effectiveness results did not show sufficient evidence that heat was removed from this region through internal conduction from the microcircuit air channels. At the midchord region, internal cooling from the microcircuit channels poses an interesting design issue. Cooling effectiveness contours point to a trade-off between film cooling and internal convection with higher blowing ratios. Higher coolant flows are

advantageous for internal heat transfer but also contribute to coolant blow-off into the mainstream. Taken as a whole, the microcircuit design proficiently cools a large portion of the blade tip aside from a small area near the trailing edge.

The data from this research will contribute to acquiring boundary conditions on the tip surface for a complete temperature distribution throughout the turbine blade. Future studies are being carried out to contribute to these boundary conditions while observing other variations of the microcircuit technology. Suggestions for further studies of the microcircuit are presented in the next section.

5.2 Recommendations for Future Work

One purpose for this research is to provide boundary conditions for a complete heat transfer analysis of the microcircuit design, but over the course of this study other issues emerged that would be interesting to pursue in future work. This study suggests that the tip leakage vortex is diminished by pressure side blowing from the microcircuit. Because the tip leakage vortex is thought to contribute to aerodynamic losses, it may be worthwhile to investigate the microcircuit influence beyond the flow measurements presented here. Further studies that measure flow planes around the vortex could verify and quantify the effect of microcircuit blowing. Aside from microcircuit effects, Hohlfeld [2003] shows that the size and location of the vortex varies with tip gap size. Experimental flow planes would provide a better description of these flow characteristics than shroud pressure distributions alone.

The nature of the microcircuit design allows for an array of modifications in exit hole shape and location, internal channel geometry, and even impingement on the tip. The presence of the dirt purge holes in the leading edge indicate that higher blowing ratios result in increased film cooling, yet these same blowing ratios may cause coolant from the microcircuit exits at the midchord to be lost to the mainstream. Because the microcircuit air passages are separated into two sections, it may be feasible to have smaller channel and exit heights at the midchord section than at the leading edge section.

This would minimize the amount of coolant blow-off at the midchord and provide a larger percentage of coolant to the leading edge.

Cooling effectiveness results give rise to a second suggestion for future work. The apparent trade-off between internal conduction and film cooling presented in this study indicates that there may be an optimal ratio of hole exit size to microcircuit channel size that allows higher velocities inside the microcircuit while maintaining lower exit velocities. Again, the goal is to limit the amount of blow-off while maximizing the amount of cooling provided by the microcircuit. These suggestions might lead to the improvement of a novel design that already appears to be an effective means of employing film cooling and internal conduction to cool the tip region.

References

Acharya, S., H. Yang, S.V. Ekkad, C. Prakash, and R. Bunker, "Numerical Simulation of Film Cooling Holes On the Tip of a Gas Turbine Blade," ASME Paper No. GT-2002-30553, 2002.

Alahyari, A., "Microcircuit Cooling Performance Experiments," Pratt & Whitney internal report, 2000.

Allen, H.W. and M.G. Kofskey, "Visualization Study of Secondary Flows in Turbine Rotor Tip Regions. NACA Technical Note 3519, 1955.

Ameri, A.A., and Bunker, R.S., "Heat Transfer and Flow on the First-Stage Blade Tip of a Power Generation Gas Turbine: Part 2 – Simulation Results," *Journal of Turbomachinery*, **122**, pp 272-277, 2000.

Barringer, M. D., Richard, O. T., Walter, J. P., Stitzel, S. M., and Thole, K. A., "Flow Field Simulations of a Gas Turbine Combustor," *Journal of Turbomachinery*, vol. 124, pp. 508-516, 2002.

Bindon, J.P., "The Measurement and Formation of Tip Clearance Loss," *Journal of Turbomachinery*, vol. 111, pg. 257-263, 1989.

Bogard, D., "Comments about the proposed blade leading edge tests," written correspondence, 2001.

Bunker, R. S., "A Review of Turbine Blade Tip Heat Transfer," Turbine 2000 Symposium on Heat Transfer in Gas Turbine Systems, Cesme, Turkey, 2000.

Bunker, R.S. and J.C. Bailey, "Effect of Squealer Cavity Depth and Oxidation on Turbine Blade Tip Heat Transfer," ASME Paper No. 2000-GT-0155, 2000.

Bunker, R.S., Bailey, J.C., and Ameri, A.A., "Heat Transfer and Flow on the First-Stage Blade Tip of a Power Generation Gas Turbine: Part 1 – Experimental Results," *Journal of Turbomachinery*, **122**, pp. 263-271, 2000.

Christophel, J.R., Master's Thesis, Dept. of Mechanical Engineering, Virginia Polytechnic Institute and State University, 2003.

Chyu, M. K., H.H. Moon, and D.E. Metzger, "Heat Transfer in the Tip Region of Grooved Turbine Blades," *Journal of Turbomachinery*, vol. 111, pg. 131-138, 1989.

Colban, W. F., "Effects of Realistic Combustor Exit Profiles on a Turbine Vane Endwall," Master's Thesis, Department of Mechanical Engineering, Virginia Polytechnic Institute and State University, 2001.

Edwards, Steve, Electronics Engineer at Aerospace Engineering Electronics Shop, Personal correspondence, 2002.

Han, J.C., J.S. Park, and C.K. Lie, "Heat Transfer and Pressure Drop in Blade Cooling Channels with Turbulence Promoters." Texas A&M University,1984 (prepared for NASA CR-3837).

IHPTET: Technology Teams in Action, Promotional Pamphlet for IHPTET (Integrated High Performance Turbine Engine Technology), Turbine Engine Division, Wright-Patterson Air Force Base.

Kim, Y. W., J.P. Downs, F.O. Soechting, W. Abdel-Messeh, G. Steuber, and S. Tanrikut, "A Summary of the Cooled Turbine Blade Tip Heat Transfer and Film Effectiveness Investigations Performed by Dr. D.E. Metzger," *Journal of Turbomachinery*, vol. 117, pg. 1-11, 1995.

Kim, Y.W. and D.E. Metzger, "Heat Transfer and Effectiveness on Film Cooled Turbine Blade Tip Models," *Journal of Turbomachinery*, vol. 117, pg. 12-21, January 1995.

Kwak, J. S. and J.C. Han, "Heat Transfer Coefficient and Film-Cooling Effectiveness on a Gas Turbine Blade Tip," ASME Paper No. GT-2002-30194, 2002a.

Kwak, J.S. and Han, J.C., "Heat Transfer Coefficient and Film-Cooling Effectiveness on the Squealer Tip of a Gas Turbine Blade," *Journal of Turbomachinery*, to be published, 2002b.

Long, John, Buildings and Ground Supervisor at Virginia Tech Physical Plant Department, Personal correspondence, 2002.

Mattingly, Jack D., *Elements of Gas Turbine Propulsion*, New York: McGraw-Hill, Inc., 1996.

Mayle, R.E., and D.E. Metzger, "Heat Transfer at the Tip of an Unshrouded Turbine Blade," 7th International Heat Transfer Conference, pg. 87-92, 1982.

Moffat, J.R., "Describing the Uncertainties in Experimental Results," *Experimental Thermal and Fluid Science*, vol. 1, pg. 3-17, 1988.

Morphis, G., and J.P Bindon, "The Effects of Relative Motion, Blade Edge Radius and Gap Size on the Blade Tip Pressure Distribution in an Annular Turbine Cascade with Clearance," ASME Paper No. 88-GT-256, 1988.

Papa, M., Goldstein, R. J., and Gori, F., "Effects of Tip Geometry and Tip Clearance on the Mass/Heat Transfer from a Large-Scale Gas Turbine Blade," *Journal of Turbomachinery*, vol. 125, pp. 90-96, 2003.

Praisner, T., Personal correspondence, 2002.

Prasad, A., "An Experimental Investigation of Tip Flows in High-Work Turbines," United Technologies Report R99-2.114.9801-1, March 1999.

Rolls-Royce, *The Jet Engine*, Derby, England: The Technical Publications Department, Rolls-Royce plc., 1992.

Santeler. K., provided computer drawing files, 2002.

Sgarzi, O., and Leboeuf, F., "Analysis of Vortices in Three-Dimensional Jets Introduced in a Cross-Flow Boundary-Layer," ASME Paper No. 97-GT-517, 1997.

Srinivasan, V., and R.J. Goldstein, "Effect of Endwall Motion on Blade Tip Heat Transfer," *Journal of Turbomachinery*, vol. 125, pp. 267-273, April 2003.

Wilson, David G, and Theodosios Korakianitis, *The Design of High Efficiency Turbomachinery and Gas Turbines*, 2nd Edition, Upper Saddle River, New Jersey: Prentice Hall, 1998.

Yamamoto, A., "Endwall Flow/Loss Mechanisms in a Linear Turbine Cascade with Blade Tip Clearance," *Journal of Turbomachinery*, vol. 111, pg. 264-275, 1989.

Yang, H., S. Acharya, S. Ekkad, C. Prakash, and R. Bunker, "Flow and Heat Transfer Predictions for a Flat-Tip Turbine Blade," ASME Paper No. GT-2002-30190, 2002.